https://satellite-navigation.springeropen.com/

# **ORIGINAL ARTICLE**

**Open Access** 

# Integrated precise orbit determination for LEO constellation and BDS-3 MEO satellites using inter-satellite links and onboard BDS-3 observations

Geer Qin<sup>1</sup>, Kecai Jiang<sup>1\*</sup>, Min Li<sup>1</sup>, Qile Zhao<sup>1</sup>, Xin Xie<sup>1</sup>, Youcun Wang<sup>2</sup>, Chao Yang<sup>3</sup>, Yubin Wang<sup>1</sup> and Chuntao Chang<sup>1</sup>

#### **Abstract**

By leveraging the high-precision spatial reference established with Global Navigation Satellite System (GNSS), we propose a low-ground-dependency and low-latency Precise Orbit Determination (POD) method employing onboard GNSS, Inter-Satellite Link (ISL) observations and readily available GNSS broadcast ephemerides, thereby reducing the need for additional ground infrastructure in the construction of Low Earth Orbit (LEO) navigation augmentation systems. By combining ISL and GNSS data from LEO satellites, this method integrated estimates the orbits of both LEO and GNSS satellites, forming a high-low unified constellation. Due to the lack of absolute spatial reference, it is inevitably subject to a common systematic rotation. To correct this, we introduce an approach that estimates the rotation angles between the coordinate system implied in the integrated GNSS POD solutions and that of the broadcast ephemerides. These angles are then used to construct rotation correction matrices and remove the systematic rotation errors from the integrated POD solutions. We validate the method using 24 BeiDou-3 Satellite Navigation System (BDS-3) Medium Earth Orbit (MEO) satellites and a LEO constellation consisting of 66 LEO satellites. After correction, the along- and cross-track orbit errors of LEO constellation decrease from 22.7 cm and 39.3 cm to 1.3 cm and 4.2 cm, respectively; for BDS-3 MEO satellites, they reduced from 124.3 and 137.8 cm to 13.2 and 13.7 cm. However, some residual error remains due to the systematic rotation inherent in the broadcast ephemerides. When this is removed, Three-Dimensional (3D) accuracy improves from 4.4 to 1.0 cm for LEO satellites, and from 19.3 to 4.6 cm for MEO satellites. As the rotation has less effect on the radial component, radial errors remain at 0.2 cm for LEO satellites and 3.4 cm for MEO satellites. Additionally, we show that, thanks to ISL connectivity, accurate POD is achievable even when only a subset of LEO satellites carries GNSS receivers. Finally, we assess the impact of using predicted Earth Rotation Parameters (ERP), and find that ERP prediction errors mainly affect the rotation correction but less the integrated POD process.

**Keywords** LEO constellation, Inter-satellite links, Constellation overall rotation, Precise orbit determination, BeiDou-3 broadcast ephemeris

\*Correspondence: Kecai Jiang kc.jiang@whu.edu.cn Full list of author information is available at the end of the article



Qin et al. Satellite Navigation (2025) 6:21 Page 2 of 21

# Introduction

In recent years, several Low Earth Orbit (LEO) satellite constellation plans have been proposed and constructed, including OneWeb, SpaceX, and CENTISPACE™ (Reid et al., 2016; Yang, 2019). These LEO constellations not only offer global broadband internet services but also can operate as independent navigation systems or to enhance existing Global Navigation Satellite Systems (GNSS) (Giorgi et al., 2019; Li et al., 2024; Reid et al., 2016; Yang et al., 2023). A key requirement for these applications is the Precise Orbit Determination (POD) of LEO constellations. For the LEO constellations equipped with Inter-Satellite Link (ISL) payloads, ISL-based ranging measurements can be used in POD processing (He et al., 2022; Homssi et al., 2022; Li et al., 2019; Lv et al., 2020; Xie et al., 2019).

The concept of ISL was first proposed and employed for Autonomous Navigation (AutoNav) in the Global Positioning System (GPS) (Ananda et al., 1990; Kur & Kalarus, 2021; Maine et al., 2003; Rajan, 2002; Rajan et al., 2003a, 2003b). It was then used in the Bei-Dou-3 Satellite Navigation System (BDS-3) and Galileo (Fernández, 2011; Ren et al., 2017; Yang et al., 2023). Numerous studies have demonstrated that ISL can significantly enhance the POD accuracy and reduce the dependency of GNSS satellites on ground stations, potentially enabling AutoNav (Cheng et al., 2023; Günther, 2018; Guo et al., 2020; Kur & Kalarus, 2021; Lv et al., 2020; Michalak et al., 2021; Tang et al., 2018; Xie et al., 2019). In addition to GNSS, ISL has also been used within LEO constellations for POD. Li et al. (2019) investigated the influence of different ISL link topologies on POD accuracy and concluded that an "all-connected" link topology can offer a superior performance. He et al. (2022) analyzed how the number and distribution of ground stations affected the POD accuracy of LEO constellations using both ISL and satellite-toground ranging measurements. They noted that a uniform global distribution with a substantial number of stations was ideal for the POD of satellite constellations. However, such an arrangement is often impractical due to geopolitical and geographical factors, as well as the high costs of construction and maintenance. This challenge is especially significant for LEO constellations, which comprise a large number of satellites with a footprint only about one-tenth that of Medium Earth Orbit (MEO) satellites. As a result, a greater number of ground stations is theoretically required (Li et al., 2024; Reid et al., 2016). When only a few or no ground stations are available for tracking the LEO constellation, relying only on ISL for POD can lead to the constellation rotating around the geocenter (Lv et al., 2020; Marz et al., 2021; Schlicht et al., 2020).

The overall rotation is primarily caused by perturbations affecting the satellites, and the inability to accurately determine the orbital orientation parameters when using only internal ranging measurements, such as ISL, in the POD process (Ananda et al., 1990; Liu, 2008; Menn & Bernstein, 1994). The perturbations in the cross-track direction of the orbital plane, such as those caused by the 12 geopotential term and solar radiation pressure, can lead to gradual changes in orbital inclination i and the Right Ascension of the Ascending Node (RAAN)  $\Omega$ , manifesting as the overall rotation of the constellation (Ananda et al., 1990; Liu, 2008). Furthermore, since ISL only provide relative measurements between satellites, it cannot detect this rotation, which is known as the rotational unobservability issue associated with ISL (Menn & Bernstein, 1994). Zhang (2005) explained that ISL can constrain orbital orientation parameters such as inclination i, argument of perigee  $\omega$ , and the different component of the change of RAAN, i.e.  $\Delta\Omega$ , for each satellite. However, they cannot constrain the same component of  $\Delta\Omega$ , which leads to the overall rotation of the constellation. Essentially, the unobservability issue of ISL arises from the rank deficiency in the design matrix used in POD processing, due to the absence of an absolute spatial reference (Li et al., 2019; Zhang, 2005).

Numerous studies have explored the methods to acquire spatial datum to address the overall rotation of satellite constellations. Rajan et al. (2003a) demonstrated that by introducing ranging measurements between ground anchor stations and satellites, the constellation's overall rotation can be effectively managed. Lv et al. (2020) utilized ISL from 21 BDS-3 satellites and two ground anchor stations and obtained POD solutions with an accuracy range of 7.0 cm to 10.0 cm. They demonstrated that two anchor stations only provide a weak constraint on orbital orientation. Ananda et al. (1990) proposed an alternative approach to control the overall rotation by constraining or fixing certain orbital orientation parameters derived from the reference ephemeris uploaded by the Operational Control Segment (OCS). For LEO constellations, Li et al. (2019) employed the a priori precise orbits of a subset of LEO Satellites (LEOs) within the constellation to constrain the orientation parameters, which can effectively control the overall rotation. Another option for obtaining spatial benchmarks is using astronomical observations. However inaccurate star sensors can lead to large POD errors of meters or even kilometers (Hong et al., 2021; Shang et al., 2018; Yu et al., 2019).

In addition to the previously mentioned methods, LEO satellites can obtain spatial datum through utilizing onboard GNSS observations in the POD process. Over the past 20 years, the use of onboard GNSS for POD was Qin et al. Satellite Navigation (2025) 6:21 Page 3 of 21

successfully validated in many LEO missions, yielding highaccuracy orbit products at precision levels of 1.0 cm to 3.0 cm (Arnold et al., 2019; Jiang et al., 2023; Montenbruck et al., 2021). For the LEO constellation, Svehla & Rothacher (2004) achieved a significant milestone by resolving the first GPS baseline in space using fixed double-difference ambiguities with onboard GPS observations from the GRACE-A/B satellites. Subsequently, the first demonstration of combined POD for a network comprising a LEO constellation and the GPS constellation was achieved using the COSMIC-1 mission, which consists of six LEO satellites (Svehla & Rothacher, 2005; Svehla, 2018). This approach enabled the simultaneous estimation of the orbits of both GPS and COSMIC-1 satellites, with the orbit of one COS-MIC-1 satellite held fixed as a reference. As for the hugescale LEO constellation, Yang (2022) employed onboard GPS observations from a LEO constellation consisting of 168 LEOs for the post-POD process, and obtained POD solutions with Three-Dimensional (3D) orbit accuracy better than 3.0 cm. This study also demonstrated that with the support of additional ground tracking stations, accuracy can be further enhanced. However, these accurate orbit products are heavily reliant on the final GNSS orbit and clock products provided by the International GNSS Service (IGS) (Hackel et al., 2017), which limits their timeliness. An alternative approach for LEOs is to use GNSS broadcast ephemeris for low-latency or even Real-Time Precise Orbit Determination (RTOD). However, due to the lower quality of broadcast ephemeris, the POD accuracy in this case can only reach the decimeter level (Montenbruck et al., 2008, 2022; Li et al., 2023a, 2023b).

In this study, we introduce a method for correcting LEO constellations' systematic rotation errors by extracting the coordinate system implied in GNSS broadcast ephemerides as the external spatial reference. This approach employs an integrated POD strategy that processes ISL and onboard BDS-3 observations from LEO satellites to simultaneously estimate the orbits of both LEO and BDS-3 MEO satellites. Due to the absence of the external spatial reference frame, the integrated POD solutions are prone to systematic rotational biases. Then this method corrects these systematic biases by referencing the relatively accurate BeiDou Coordinate System (BDCS) implied in the readily available BDS-3 broadcast ephemerides (Liu et al., 2019). In this paper, we employ the BDS-3 MEO Satellites (MEOs) for validating the feasibility of the method and it is worth noting that we focus solely on constellation rotation, no translation effects.

This paper is organized as follows: Sect. 2 presents the observation models and the basic principles of this rotation correction method. Section 3 describes the employed LEO constellation simulation and the POD strategies. Section 4 provides a comprehensive analysis of

the feasibility and the effectiveness of this rotation correction method. Finally, detailed summaries are drawn.

#### Models and method

In this section, we first introduce the observation models of ISL and onboard BDS-3 measurements used in the integrated POD process. We then detail the principles and methodology of the constellation rotation correction for mitigating systematic rotation errors in the integrated orbit determination of LEOs and BDS-3 MEOs.

#### Observation models

The undifferenced Ionospheric-Free (IF) (Montenbruck et al., 2018) combinations of onboard BDS-3 dual frequency code and carrier phase observations are adopted in the integrated POD processing. The IF combinations can be expressed as follows:

$$P_{\text{LEO},j,\text{IF}}^{\text{C}} = |\mathbf{R}_{\text{MEO}} - \mathbf{R}_{\text{LEO}}| + t_{\text{LEO}} - t^{\text{C}} + \varepsilon_{\text{LEO},j}^{\text{C,P}}$$
 (1)

$$L_{\text{LEO},j,\text{IF}}^{\text{C}} = |\mathbf{R}_{\text{MEO}} - \mathbf{R}_{\text{LEO}}| + t_{\text{LEO}} - t^{\text{C}} + \lambda \widetilde{N}_{\text{LEO},j,\text{IF}}^{\text{C}} + \varepsilon_{\text{LEO},j}^{\text{C,L}}$$
(2)

In this paper, we employ B1C and B2a frequency of BDS-3.  $P_{\text{LEO},j,\text{IF}}^{\text{C}}$  and  $L_{\text{LEO},j,\text{IF}}^{\text{C}}$  are the IF combinations of code and carrier phase observations at epoch t. Superscript C refers to the BDS-3 and subscript LEO and j represent the LEO satellites and carrier frequency, respectively.  $|R_{\text{MEO}} - R_{\text{LEO}}|$  is the geometrical distance between BDS-3 MEOs and LEOs.  $t_{\text{LEO}}$  and  $t^{\text{C}}$  are clock offsets of LEOs and BDS-3 MEOs in meters, respectively.  $\lambda \widetilde{N}_{\text{LEO},j,\text{IF}}^{\text{C}}$  means the IF carrier phase ambiguity in meters.  $\varepsilon_{\text{LEO},j}^{\text{C}}$  and  $\varepsilon_{\text{LEO},j}^{\text{C}}$  donate code and carrier phase observation errors, respectively.

For the ISL ranging measurements, the dual one-way ranging mode is employed and the original observation models of a pair of forward and backward ranging measurements are expressed as follows (Xie et al., 2019):

$$P_{\text{LEO}_{AB}}(t_{1}) = \left| \mathbf{R}_{\text{LEO}_{A}}(t_{1}) - \mathbf{R}_{\text{LEO}_{B}}(t_{1} - t_{1}) \right|$$

$$+ c \left[ t_{\text{LEO}_{A}}(t_{1}) - t_{\text{LEO}_{B}}(t_{1} - t_{1}) \right]$$

$$+ c \left( d_{\text{LEO}_{B}}^{\text{send}} + d_{\text{LEO}_{A}}^{\text{rec}} \right) + b_{\text{LEO}_{AB}}$$

$$+ \varepsilon_{\text{LEO}_{AB}}$$

$$(3)$$

$$P_{\text{LEO}_{\text{BA}}}(t_2) = \left| \mathbf{R}_{\text{LEO}_{\text{B}}}(t_2) - \mathbf{R}_{\text{LEO}_{\text{A}}}(t_2 - t_2) \right|$$

$$+ c \left[ t_{\text{LEO}_{\text{B}}}(t_2) - t_{\text{LEO}_{\text{A}}}(t_2 - t_2) \right]$$

$$+ c \left( d_{\text{LEO}_{\text{A}}}^{\text{send}} + d_{\text{LEO}_{\text{B}}}^{\text{rec}} \right) + b_{\text{LEO}_{\text{BA}}}$$

$$+ \varepsilon_{\text{LEO}_{\text{BA}}}$$

$$(4)$$

Qin et al. Satellite Navigation (2025) 6:21 Page 4 of 21

where  $P_{\mathrm{LEO_{AB}}}(t_1)$  and  $P_{\mathrm{LEO_{BA}}}(t_2)$  are forward and backward ranging observations received by LEO satellites A and B at epoch  $t_1$  and  $t_2$ , and  $\Delta t_1$  and  $\Delta t_2$  are signal propagation time, respectively.  $R_{\mathrm{LEO_A}}$  and  $R_{\mathrm{LEO_B}}$  are the phase centers of the terminals transmitting or receiving the ranging signals of LEO satellite A and B at a certain epoch.  $t_{\mathrm{LEO_A}}$  and  $t_{\mathrm{LEO_B}}$  are their satellite clock offsets, respectively.  $d_{\mathrm{LEO_A}}^{\mathrm{send}}$  and  $d_{\mathrm{LEO_B}}^{\mathrm{send}}$  donate the transmitting hardware delay and  $d_{\mathrm{LEO_A}}^{\mathrm{rec}}$  and  $d_{\mathrm{LEO_B}}^{\mathrm{rec}}$  represent the receiving hardware delay, respectively. c is the speed of light.  $b_{\mathrm{LEO_{AB}}}$  and  $b_{\mathrm{LEO_{BA}}}$  are some systematic errors, such as relativistic effects and gravitational time delay.  $\varepsilon_{\mathrm{LEO_{AB}}}$  and  $\varepsilon_{\mathrm{LEO_{BA}}}$  are ranging noises.

In the integrated POD process, the Clock-Free (CF) combined observation which is transformed to epoch  $t_0$  (Xie et al., 2019) is processed. It is expressed as follows:

$$P_{\text{LEO}_{AB},\text{CF}}(t_0) = \frac{P_{\text{LEO}_{AB}}(t_0) + P_{\text{LEO}_{BA}}(t_0)}{2}$$

$$= \left| \mathbf{R}_{\text{LEO}_{B}}(t_0) - \mathbf{R}_{\text{LEO}_{A}}(t_0) \right|$$

$$+ c \left( D_{\text{LEO}_{A}} + D_{\text{LEO}_{B}} \right)$$

$$+ \frac{b_{\text{LEO}_{AB}} + b_{\text{LEO}_{BA}}}{2} + \varepsilon_{\text{CF}}$$
where
$$D_{\text{LEO}_{A}} = \frac{\left( d_{\text{LEO}_{A}}^{\text{send}} + d_{\text{LEO}_{A}}^{\text{rec}} \right)}{2} \quad \text{and}$$

 $D_{\rm LEO_B} = \frac{\left(d_{\rm LEO_B}^{\rm send} + d_{\rm LEO_B}^{\rm rec}\right)}{2} \mbox{ are half of the sum of sendingend and receiving-end hardware delays of satellite A and B, respectively. They are estimated as constant parameters with orbit parameters. The detailed transformation procedures from Eq. (3) and Eq. (4) to Eq. (5) can refer to Xie et al. (2019) and Lv et al. (2020).$ 

# Rotation correction method

For the rotation correction method, an integrated POD approach is first employed to process ISL and onboard BDS-3 observations from LEOs, and the orbits of LEOs and BDS-3 MEOs are simultaneously estimated, which forms a unified high-low constellation consisting of the LEO constellation and BDS-3 MEOs as illustrated in Fig. 1. Since there is no direct observation between this unified constellation and the ground network, it is hard to obtain an absolute spatial reference from the ground. Moreover, the observations used in the integrated POD process consist solely of internal ranging measurements within this unified constellation, generating a rotational unobservability issue. This inevitably results in a systematic rotation of the entire unified constellation.

This systematic rotation manifests as the rotation of the coordinate system implied in the integrated POD solutions relative to the BeiDou Coordinate System, as depicted in Fig. 2. This systematic rotation arises from the rank deficiency of the normal equation employed in

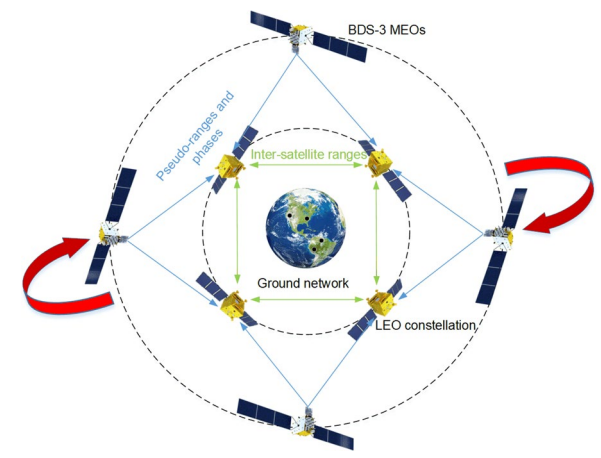


**Fig. 1** The unified constellation consisting of the LEO constellation and the BDS-3 MEOs with the connection through ISL and onboard BDS-3 observations from the LEOs

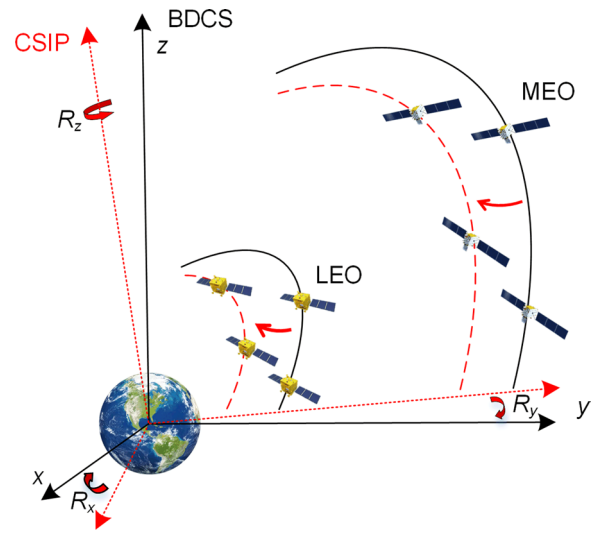


**Fig. 2** The overall rotation of the coordinate system implied in the integrated POD solutions (CSIP) with respect to the BeiDou Coordinate System (BDCS)

the parameter estimation process. To address this rank deficiency, this method utilizes the positions of BDS-3 MEOs derived from BDS-3 broadcast ephemerides to construct virtual observation equations. These virtual observations then participate in building the normal equations for providing loose constraints. However, this process only offers a coarse spatial reference and is insufficient to fully align the coordinate system implied in the integrated POD solutions with the BDCS realized by the BDS-3 broadcast orbits, leaving the integrated POD solutions still containing systematic rotation errors. Then this rotation correction method applies the Helmert

Qin et al. Satellite Navigation (2025) 6:21 Page 5 of 21

transformation, as shown in Eq. (6) (Boucher et al., 2001, Nicolini & Caporali, 2018) and use the BDCS implied in the BDS-3 broadcast ephemerides as the reference to quantify and correct these systematic rotation errors.

$$\begin{pmatrix} X_2 \\ Y_2 \\ Z_2 \end{pmatrix} = \begin{pmatrix} 1 & R_z & -R_y \\ -R_z & 1 & R_x \\ R_y & -R_x & 1 \end{pmatrix} \bullet \begin{pmatrix} X_1 \\ Y_1 \\ Z_1 \end{pmatrix}$$
(6)

Figure 3 presents the flowchart of our rotation correction method. Since the integrated POD processing is typically performed in the Earth-Centered Inertial (ECI) coordinate system, the resulting integrated POD solutions are expressed in ECI. However, the BDS-3 broadcast ephemerides are generally provided in the Earth-Centered Earth-Fixed (ECEF) coordinate system. In this study, we transform the broadcast ephemeris from ECEF to ECI and use them as the spatial reference for subsequent rotation correction of the integrated POD solutions. As shown in Fig. 3, the broadcast ephemeris is first converted from ECEF to ECI. Subsequently, a set of rotation angles in radians, denoted as  $R_x$ ,  $R_y$  and  $R_z$ , representing systematic rotations of the coordinate system of the integrated POD solutions around the x-, y-, and z- axes of the BDCS (as illustrated in Fig. 2), are derived using Eq. (6), where  $(X_2, Y_2, Z_2)^T$  and  $(X_1, Y_1, Z_1)^T$  denote the positions of the BDS-3 MEOs derived from the broadcast ephemerides and the integrated POD solutions, respectively. These determined rotation angles are then used to construct a rotation correction matrix. In the subsequent rotation correction, this matrix is applied to the position vectors  $(X_1, Y_1, Z_1)^T$ , representing the integrated POD solutions of both the BDS-3 MEOs and LEO constellation, yielding the rotation-corrected positions of the unified constellation, denoted as  $(X_2, Y_2, Z_2)^T$ , thereby completing the rotation correction process. As shown in Fig. 1, this method relies solely on LEO satellite's onboard observations and can obtain space reference from the relatively accurate and readily available BDCS implied by the BDS-3 broadcast ephemeris, significantly reducing the dependence of the LEO constellation POD on the distribution and number of ground tracking stations, while enabling faster and more efficient orbit determination.

# **Data and strategies**

Since no real ISL or onboard BDS-3 observations from the LEO constellation are available, they are simulated for demonstration and analysis. This section introduces the LEO constellation and observation simulation process. We then discuss two POD strategies designed to support our analytical work.

# LEO constellation and onboard data simulation

In the simulation process, the orbits of the LEOs and BDS-3 MEOs are known in advance. For the BDS-3 MEOs, we directly employ the precise orbit products provided by GeoForschungsZentrum (GFZ). For the LEOs, a Walker constellation (975 km, 99.8°: 66/6/2) is simulated. This LEO constellation comprises 66 LEOs, operating at an orbital altitude of 975 km with an inclination of 99.8°. These satellites are distributed in 6 equally

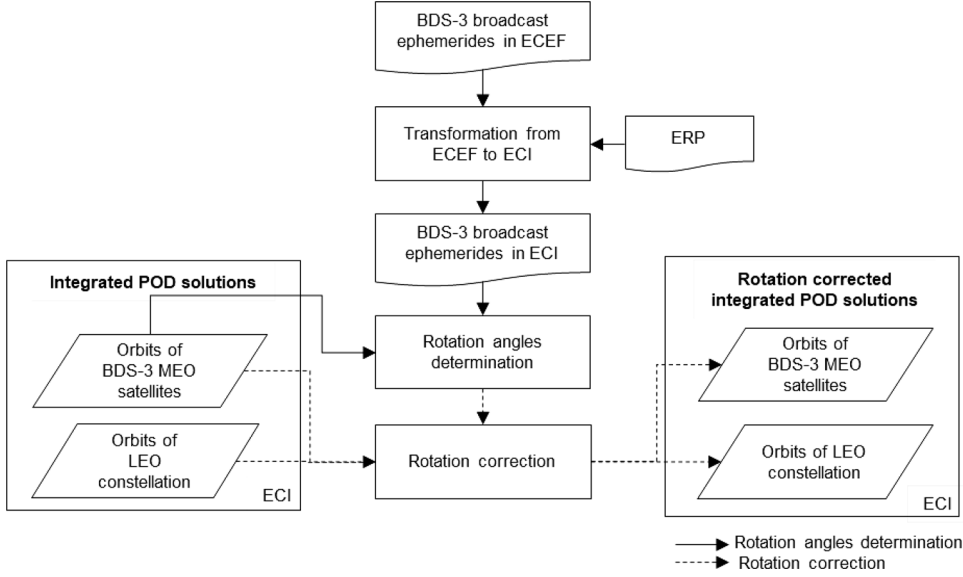


Fig. 3 Flowchart of the rotation correction method

Qin et al. Satellite Navigation (2025) 6:21 Page 6 of 21

spaced orbitals and the relative spacing between satellites in adjacent planes is 2. The Position And Navigation Data Analyst (PANDA) software, developed by Wuhan University (Liu & Ge, 2003), is used to generate their orbits based on the strategies and dynamical models listed in Table 3. The orbits of the LEOs and BDS-3 MEOs will also be used to assess the accuracy of the POD solution and thus referred to as the true orbits.

For simulating onboard BDS-3 observations, the ionospheric delay is neglected due to the use of IF combinations. The geometrical distance between the LEOs and BDS-3 MEOs is computed using their true orbits. The antenna products of IGS are applied for Phase Center Offset (PCO) correction of the BDS-3 MEOs, while the corrections for the onboard LEO receivers are set to zero. The clock offsets for both BDS-3 MEOs and LEOs are derived directly from the GFZ precise clock products. The clock offsets of BDS-3 MEOs are got based on their Pseudo-Random Noise (PRN) numbers, while the clock offsets for the LEOs are simulated using the receiver clock offsets of the ground tracking stations (Yang, 2022). For ambiguity resolution, an integer  $N_{\text{LEO},i}^{\text{C}}$  is assigned to each continuous arc for each frequency, and in the POD process, the ionospheric-free combinations of ambiguity  $\widetilde{N}_{\mathrm{LEO},j,\mathrm{IF}}^{\mathrm{C}}$  is processed. Finally, the noise in code and phase observations, denoted as  $\varepsilon_{\mathrm{LEO},j}^{\mathrm{C,P}}$ ,  $\varepsilon_{\mathrm{LEO},j}^{\mathrm{C,L}}$  is simulated as random values following a normal distribution with zeromean and Standard Deviations (STD) of 5.0 mm and 1.0 m, respectively (Li et al., 2019). The detailed simulation strategies are presented in Table 1.

To simulate ISL ranging measurements, we adopt the "4-connected" topology (He et al., 2022), as illustrated in Fig. 4. This topology enables each LEO satellite in the constellation to maintain continuous connections with two neighboring satellites in the same orbital plane, as well as with the satellites in the two adjacent orbital planes. Referring to the BDS-3 ISL observations (Xie et al., 2019), we similarly establish each pair of ISL within a time frame of 3.0 s. This means that the forward-ranging observation

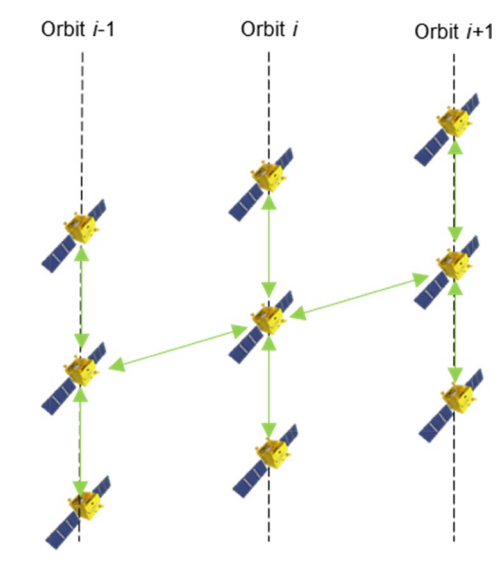


Fig. 4 "4-connected" ISL topology

is completed in the first 1.5 s, followed by a backward-ranging observation in the subsequent 1.5 s.

The ISL ranging measurements are simulated based on the original ISL observation models expressed by Eqs. (3) and (4). The phase centers of the antennas transmitting and receiving the ranging signals, denoted as  $R_{LEO_A}$  and  $R_{\rm LEO_B}$ , are simplified as the center of mass of the LEOs derived from their simulated true orbits. The simulation methods for the satellite clock offsets  $t_{LEO_A}$  and  $t_{LEO_B}$  are consistent with those used for the onboard BDS-3 receivers. Given that the hardware delays of Ka-band signals are relatively stable (Xie et al., 2019), the hardware delays  $d_{\mathrm{LEO_A}}^{\mathrm{send}}$  and  $d_{\mathrm{LEO_B}}^{\mathrm{send}}$ , of transmitting devices as well as the hardware delays  $d_{\mathrm{LEO_A}}^{\mathrm{rec}}$  and  $d_{\mathrm{LEO_B}}^{\mathrm{rec}}$ , of receiving devices are simulated as small constant values. For the systematic errors  $b_{
m LEO_{AB}}$  and  $b_{
m LEO_{BA}}$ , we consider only the relativistic effects, simulated using existing models. Based on the findings by Xie et al. (2019), the ranging noise for BDS-3 ISL observations is less than 10.0 cm. Considering the more complex space environment where the LEOs operate, we amplify the ranging noises  $\varepsilon_{\text{LEO}_{AB}}$  and  $\varepsilon_{\text{LEO}_{BA}}$  as

**Table 1** Simulation strategies for the code and phase observations

Items	Simulation strategies		
R <sub>MEO</sub> , R <sub>LEO</sub>	Using the simulated true orbits of LEOs and BDS-3 MEOs		
$t_{LEO}$	Clock offsets of ground stations from the precise clock products of the GFZ		
$t^{C}$	Clock offsets of BDS-3 MEOs from the precise clock products of the GFZ		
IC LEO,j	Neglect as the adaptation of the IF combinations		
NC LEO,	One integer for each continuous arc		
$\varepsilon_{\text{LEO},j}^{\text{C,P}}, \varepsilon_{\text{LEO},j}^{\text{C,L}}$	Random values obeying zero-mean normal distribution with 1.0 m and 5.0 mm standard STD		

Qin et al. Satellite Navigation (2025) 6:21 Page 7 of 21

**Table 2** Summary of the POD processing strategies

Strategies	Employed observations
1	ISL, BDS-3 data from all LEOs
2	ISL, BDS-3 data provided by part of LEOs

zero-mean normal distributions with a standard deviation of 15.0 cm.

# POD processing strategies

Two POD processing strategies are designed and summarized in Table 2, both following the method described in Sect. 2.2. Strategy 1 uses ISL and onboard BDS-3 observations from all LEO satellites to first demonstrate the phenomenon of overall constellation rotation and then evaluate the performance of the proposed rotation correction method. Strategy 2 is developed to assess the feasibility of the method in the scenarios where only a subset of LEO satellites provides onboard BDS-3 observations.

The entire POD processing period spans from Day of Year (DOY) 277 to 291, 2022. All data are processed using a modified version of the PANDA software package. Each day is treated as an independent POD arc, and the data are processed in batch mode. As this study focuses on the systematic rotation errors of LEO constellations, to avoid introducing additional biases that can affect the validation of the introduced rotation correction method, the same dynamical models used to generate the LEO true orbits are also adopted in POD processing. For BDS-3 MEOs, the differences between the dynamical models used in PANDA and those used by GFZ may lead to centimeter-level biases in the POD results.

For the two processing strategies, the IF combinations of B1C and B2a code and carrier-phase observations are employed. The onboard BDS-3 observations are processed at a 30 s sampling rate. The a priori standard deviations for the raw code and carrier phase observations are set to 1.0 m and 5.0 mm, respectively. For the ISL ranging measurements, the CF combinations are used, with the same 30 s sampling interval. The a priori standard deviation for ISL observations is set to 15.0 cm.

The estimated parameters for each BDS-3 MEO satellite include the initial position and velocity, five Solar Radiation Pressure (SRP) parameters of the ECOM model, and an empirical along-track parameter (Guo, 2014). Additionally, one BDS-3 MEO satellite's clock is used as a reference, while the clock offsets for the remaining BDS-3 MEOs and the onboard BDS-3 receivers of all LEOs are estimated. For each LEO satellite, in addition to the initial position, velocity, and onboard BDS-3 receiver's clock offsets, one SRP scale parameter per arc and piecewise atmospheric drag parameters as well as

the amplitudes of Circle-Per-Revolution (CPR) empirical acceleration of sine and cosine acting in the along-track and cross-track directions are also estimated. Furthermore, one constant parameter of the sum of ISL sendingend and receiving-end hardware delay of each LEOs are also estimated (Xie et al., 2019).

Besides, Earth Rotation Parameters (ERP) are essential for the transformations between the Earth- ECEF and ECI coordinate systems. In this paper, the observed ERP from the International Earth Rotation and Reference System Service (IERS) Bulletin B is employed in the observation simulation process. Then in the introduced rotation correction method, ERP is first used in the integrated POD process conducted in the ECI and is subsequently employed to transform GNSS broadcast ephemerides from the ECEF into the ECI for rotation correction as illustrated in Fig. 3. In the analysis sections of this paper, we first use the observed ERP from IERS Bulletin B to conduct the two POD strategies for comprehensively evaluating the performance of the introduced rotation correction method. However, under certain POD operational constraints, observed ERP may be unavailable. In such cases, predicted ERP is utilized for both integrated POD and rotation correction. To assess the impact of ERP prediction errors on the performance of the introduced method, we will conduct the Strategy 1 again using the predicted ERP from IERS Bulletin A. Table 3 summarizes the detailed processing strategies employed in POD process.

# **Results and analysis**

For Strategy 1, we first analyzes the integrated POD results of the unified constellation under the influence of rotation errors and then evaluates the feasibility and performance of the introduced rotation correction method. Then with Strategy 2, the method's performance is further demonstrated in the scenarios where only a subset of LEO satellites provides onboard BDS-3 observations. Finally, the impact of employing predicted ERP on this rotation correction method's effectiveness is examined.

# Analysis of the constellation's overall rotation

To perform rotation correction, three rotation angles  $R_x$ ,  $R_y$  and  $R_z$  need determining first. These angles quantify the rotation of the coordinate system implied by the integrated POD solutions relative to that implied by the true orbits of the unified constellation, characterizing the constellation's overall rotation. To demonstrate the systematic rotation errors contained in the integrated POD solutions, we first determine these rotation angles with the true orbits of the unified constellation as reference. As shown in Fig. 5, it indicates significant systematic rotations around all three axes of the integrated POD

Qin et al. Satellite Navigation (2025) 6:21 Page 8 of 21

**Table 3** Dynamic models, observation models and estimated parameters used for integrated precise orbit determination

Dynamic models	Description			
Conventional inertial reference frame	Geocentric celestial reference frame at J2000.0			
Gravity model	EIGEN_5C, 120 × 120 for LEOs, 12 × 12 for BDS-3 MEOs (Shako et al., 2014)			
Solid earth & pole tides	IERS 2010 conventions (Petit & Luzum, 2010)			
Ocean tides	Finite Element Solution (FES2004) (30 $\times$ 30) (Lyard et al., 2006)			
N-body disturbance	JPL DE405 (Standish & Williams, 1992)			
Relatively	IERS Conventions 2010 (Petit & Luzum, 2010)			
Solar radiation	Box-wing model for LEOs (Marshall & Luthcke, 1994); Extended CODE Orbit Model (I model (Springer et al., 1999)	ECOM) 5-parameter		
Atmospheric drag	Box-wing model, atmospheric density adopts DTM-2013 (Bruinsma, 2015) for LEOs; I	None for MEOs		
Empirical acceleration	Piecewise periodic terms			
Earth Rotation Parameters	Observed ERP for observation simulation; Both observed and predicted ERP for analysis	ysis (Dick & Richter, 2004)		
Observation models	Onboard BDS-3 obs	ISL		
Observation	Undifferenced IF code and carrier-phase combinations	CF combinations		
POD arc length	1 d			
Sampling interval	30 s			
Elevation mask	10 °	Ignore		
Prior accuracy	Code: 1.0 m; phase: 5.0 mm	15.0 cm		
Estimated parameters	Description			
Initial states	Positions and velocity at the initial epoch of LEOs and BDS-3 MEOs			
Clock offset	Each epoch as white noise for each LEOs and BDS-3 MEOs; C25 is selected as the refere	ence clock;		
Ambiguity	Adjusted as float constant values for each continuous arc if BDS-3 data of LEOs being p	processed		
Hardware delay of ISL	One constant parameter per arc of the sum of ISL sending-end and receiving-end hard	dware delay of each LEOs		
Atmosphere drag	One per 120 min only for LEOs			
Solar radiation	One per day for LEOs; Five per day for BDS-3 MEOs			
Empirical accelerations	Estimating amplitudes of circle-per-revolution empirical acceleration of sine and cosin and cross-track directions for each LEO satellite; one per day constant empirical accele direction for each BDS-3 MEO satellite			

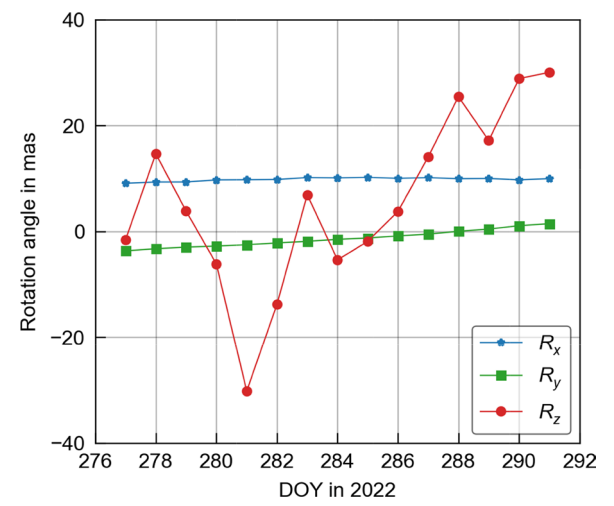


**Fig. 5** Daily systematic rotation angles  $R_x$ ,  $R_y$  and  $R_z$  of the coordinate system implied in the integrated POD solutions relative to the coordinate system implied in the true orbits of the unifed constellaion throughout the analysis period

solutions, with the most pronounced rotation occurring about the z-axis. Over the entire simulation period, the mean absolute value and STD of  $R_z$  reach  $135.8 \times 10^{-1}$  milliarcsecond (mas) and  $160.2 \times 10^{-1}$  mas, respectively. This observation aligns with the explanation by Zhang (2005), which states that internal constellation ranging is insufficient to constrain the common part of variations in RAAN. In contrast, the rotations around the x- and y-axes are smaller, owing to partial inclination correction afforded by inter-orbit ranging measurements (Liu, 2008; Zhang, 2005). The average absolute values of  $R_x$  and  $R_y$  are  $98.3 \times 10^{-1}$  mas and  $17.4 \times 10^{-1}$  mas, with STDs of  $3.2 \times 10^{-1}$  mas and  $15.5 \times 10^{-1}$  mas, respectively.

Figure 6 illustrates the daily Root-Mean-Square (RMS) orbit errors of the integrated POD solutions for the LEO constellation and BDS-3 MEOs. Due to the influence of the constellation's overall rotation, the integrated POD solutions exhibit significant deviations in the along-track and cross-track directions. Moreover, given the higher orbital altitude of BDS-3 satellites, a rotation of the same

Qin et al. Satellite Navigation (2025) 6:21 Page 9 of 21

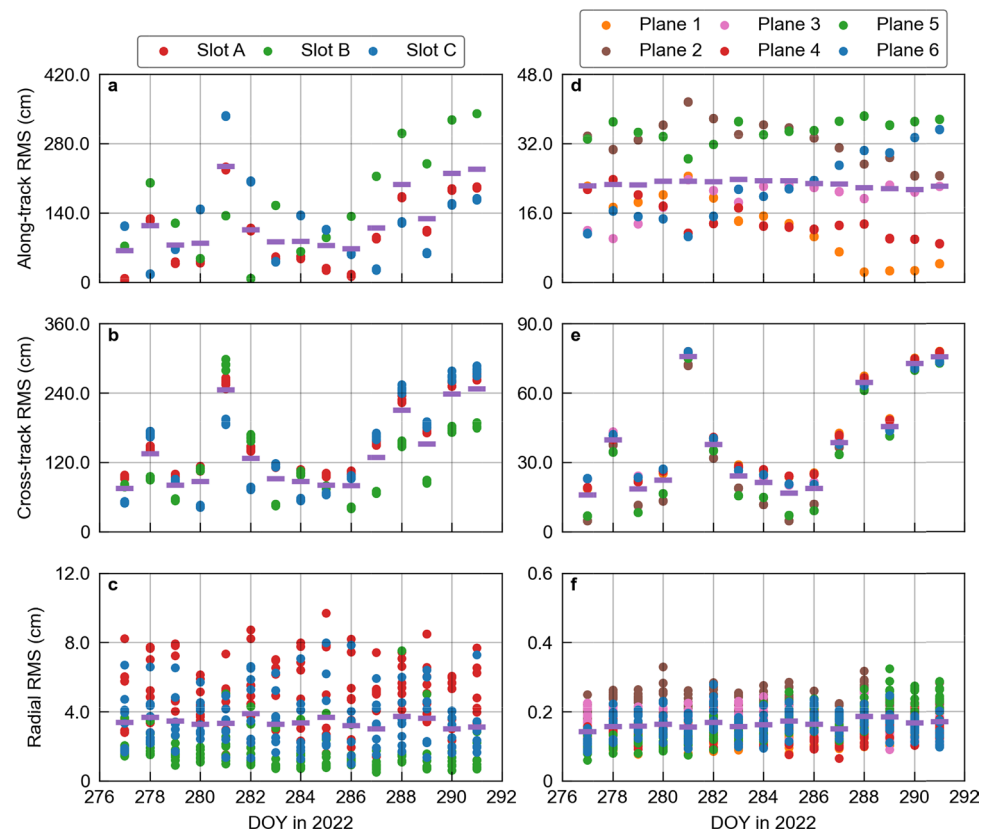


**Fig. 6** Daily RMS orbit errors of the integrated POD solutions of BDS-3 MEO satellites **a, b, c** and the LEO constellation **d, e, f** in the along-track, cross-track, and radial directions. Each dot represents the daily RMS orbit errors of each LEO and BDS-3 MEO satellites, with different colors distinguishing satellites in various orbital planes. The purple short dash indicates the daily constellation averaged RMS orbit errors

magnitude induces larger orbital deviations in BDS-3 MEOs compared to LEOs. The average daily RMS orbit errors for LEOs are 22.7 cm and 39.3 cm in the along-track and cross-track directions, respectively, while those for BDS-3 MEOs reach 124.3 and 137.8 cm. In contrast, the orbital errors in the radial direction are relatively small, with the averaged daily RMS values of 3.4 cm for BDS-3 MEOs and 0.2 cm for LEOs.

Figure 6 shows that the same-colored dots, representing the daily RMS orbit errors of each LEO and BDS-3 MEO satellite within the same orbital plane, tend to cluster in the along-track and cross-track directions. This pattern indicates that the satellites in the same orbital plane are similarly influenced by the constellation's overall rotation. Notably, significant rotation about the z-axis, as shown in Fig. 5, induces substantial orbital deviations across all orbital planes of both LEOs and BDS-3 MEOs. The projections of these deviations onto the along-track and cross-track directions become the dominant contributors to the errors in these components, making the orbit errors variations in along- and cross-track orbit errors for each orbital plane either follow or inversely reflect the

oscillatory behavior of  $R_z$  depicted in Fig. 5. Besides, the differences in the equatorial-plane positions of the LEO and BDS-3 MEO orbital planes lead to varying responses to the constellation's rotation around the x- and y-axes, likely explaining the observed inter-plane inconsistencies in orbit errors, especially in the along-track direction.

The constellation's overall rotation mainly effects the orbital inclination i and the RAAN  $\Omega$  of each orbit plane of the unified constellation (Xia et al., 2024). To investigate the impact of the systematic rotation errors on these orientation parameters within J2000 ECI coordinate system, we take the integrated POD solutions of the LEO constellation on DOY 291, 2022 as an example and plot the errors of the orbital inclination i and the RAAN  $\Omega$  of each LEO satellite in each orbit plane in the Fig. 7. Moreover, the corresponding time series of constellation's rotation angles  $R_{xy}$   $R_{y}$  and  $R_{z}$  are plotted in Fig. 8.

In Fig. 7, benefiting from the constraints provided by intra- and inter-orbit ISL, the variation patterns of the orbital inclination i and the RAAN  $\Omega$  for each LEO satellite in the same orbital plane are generally consistent (Xia et al., 2024; Zhang, 2005). However, notable systematic

Qin et al. Satellite Navigation (2025) 6:21 Page 10 of 21

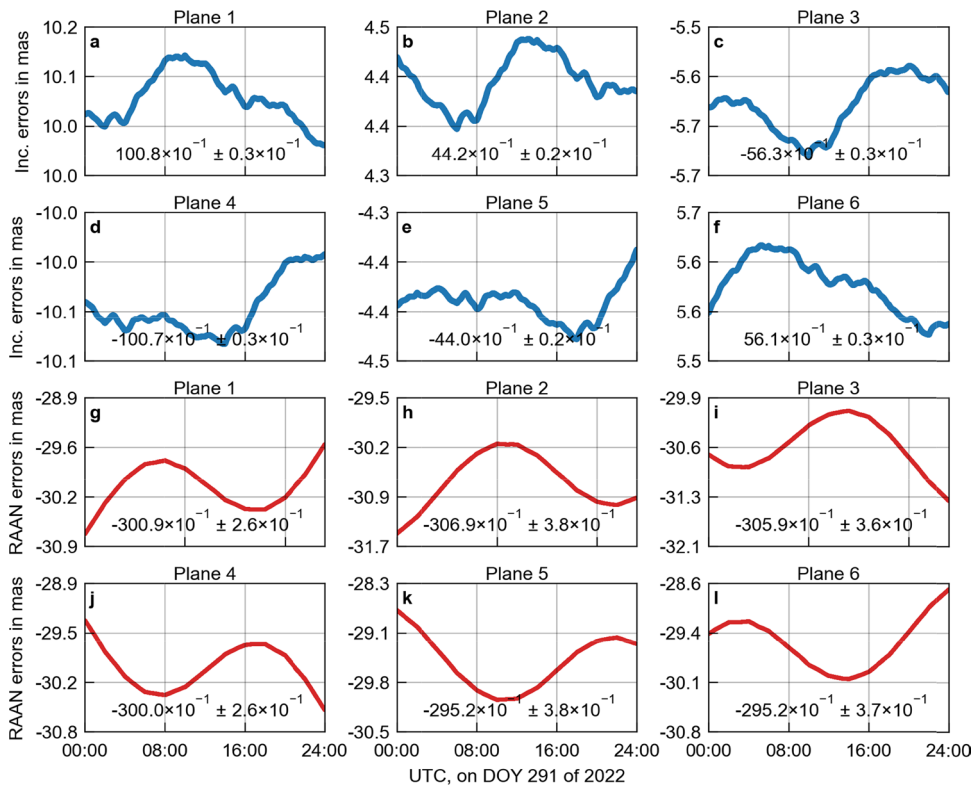


Fig. 7 Time series of the errors of orbital inclination (Inc.) i a-f and the Right Ascension of the Ascending Node (RAAN)  $\Omega$  g-l of each LEO satellite in different orbit planes within the LEO constellation. The mean values and standard deviations of the errors of orbital inclination and RAAN of each orbit plane of the LEO constellation are shown in the bottom of each subplot in mas

errors are observed in both the orbital inclination i and the RAAN  $\Omega$ . For inclination i, the systematic errors vary across orbital planes, with the magnitudes comparable to the systematic rotations about the *x*- and *y*-axes, i.e.  $R_x$  and  $R_y$ , but much smaller than  $R_z$ , as shown in Fig. 8. This suggests that inclination errors are primarily caused by the constellation's rotation around the x- and y-axes. Besides, the orbital planes at different RAAN  $\Omega$ have different angles relative to the x- and y-axes, leading to the different impacts of the constellation's overall rotation around these two axes on the changes of inclination across the various planes. As a result, the systematic errors in the orbital inclination i differ for orbital planes located at different RAAN  $\Omega$ , which corresponds to the aforementioned noticeable inconsistencies in orbit errors across different planes in the along-track component. Moreover, from Fig. 7a-f, the systematic errors in the orbital inclination i across different orbital planes range from  $-100.7 \times 10^{-1}$  mas to  $100.8 \times 10^{-1}$  mas. The simulated LEO constellation consists of six orbital planes evenly distributed around the equatorial plane, with each plane's RAAN  $\Omega$  differing by 60°. Consequently, the absolute values of the systematic errors in inclination for two orbital planes with the RAAN  $\Omega$  differing by 180° are essentially similar. For the systematic biases in RAAN  $\Omega$ , from the Fig. 7g–l, they reach approximately 30.0 mas, which aligns with the magnitudes of  $R_z$  shown in Fig. 8. This indicates that RAAN variations are predominantly governed by rotation about the z-axis, causing uniform precession of orbital planes within the equatorial plane.

# Performance of the rotation correction method

Following the analysis of the overall rotation issue, the systematic rotation errors contained in the integrated POD solutions are corrected using the rotation correction method. First, the rotation-corrected POD results for the LEO constellation on DOY 283 and 291 are employed to assess the improvements in the systematic errors of orbital inclination i and RAAN  $\Omega$ . Figure 9 presents the residual errors in orbital inclination i and RAAN  $\Omega$  of each orbit plane of the LEO constellation and their mean values and standard deviations are summarized in Table 4 and Table 5. Besides, Fig. 9 also shows the residual rotation angles of the coordinate system implied in the corrected integrated POD solutions relative to that of the true orbits. As shown in Fig. 9, on DOY 291, 2022, the rotation angles  $R_x$ ,  $R_y$  and  $R_z$  decrease substantially from  $99.6 \times 10^{-1}$  mas,  $14.7 \times 10^{-1}$  mas, and

Qin et al. Satellite Navigation (2025) 6:21 Page 11 of 21

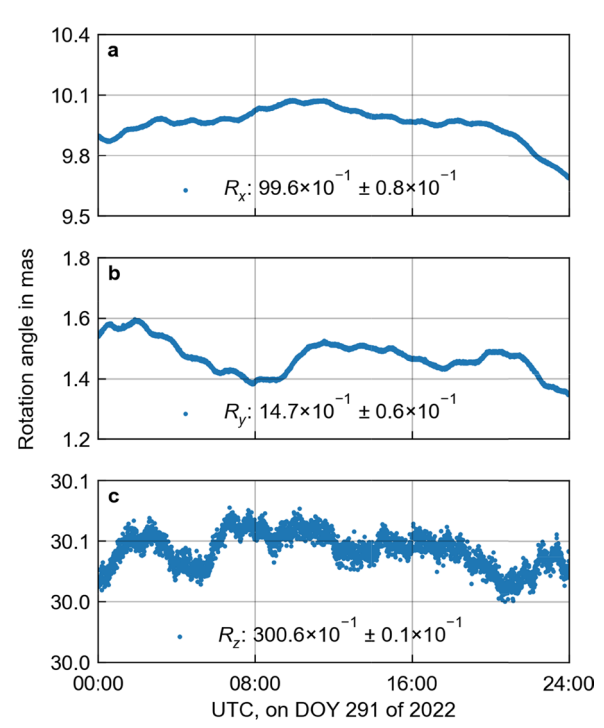


**Fig. 8** Time series of the LEO constellation's rotation angles  $R_x$ ,  $R_y$  and  $R_z$  on DOY 291, 2022. The mean values and standard deviations of these rotation angles are shown in the bottom of each subplot in mas

 $300.6 \times 10^{-1}$  mas, as shown in Fig. 8, to  $-1.2 \times 10^{-1}$  mas,  $-4.6 \times 10^{-1}$  mas, and  $-54.2 \times 10^{-1}$  mas, respectively. On DOY 283, the corresponding rotation angles are -2.7 $\times 10^{-1}$  mas,  $-2.7 \times 10^{-1}$  mas, and  $-6.1 \times 10^{-1}$  mas. Correspondingly, the systematic errors in both inclination i and RAAN  $\Omega$  are markedly reduced. For instance, the maximum systematic error in inclination i is reduced from  $100.8 \times 10^{-1}$  mas to  $1.8 \times 10^{-1}$  mas, while for RAAN  $\Omega$ , the maximum error in orbital plane 2 decreases from  $306.9 \times 10^{-1}$  mas to  $53.6 \times 10^{-1}$  mas. These results indicates that the correction method effectively mitigates the systematic constellation rotation. Besides, the inconsistencies of the systematic errors in the orbital inclination i of different orbital planes located at different RAAN  $\Omega$ is also significantly eliminated, which indicates that the inconsistencies in orbit errors across different planes in the along-track direction are caused by the constellation's rotation and can also be improved after rotation correction.

However, as shown in Fig. 9 (f), residual rotation errors in  $R_z$ , reaching nearly 5.4 mas, are evident on DOY 291, whereas no significant residual rotation is observed on DOY 283. This may be attributed to the inherent systematic rotation errors contained in the broadcast ephemeris (Chen et al., 2021; Li et al., 2023c). To validate this, the precise ephemerides from GFZ are used as a reference to

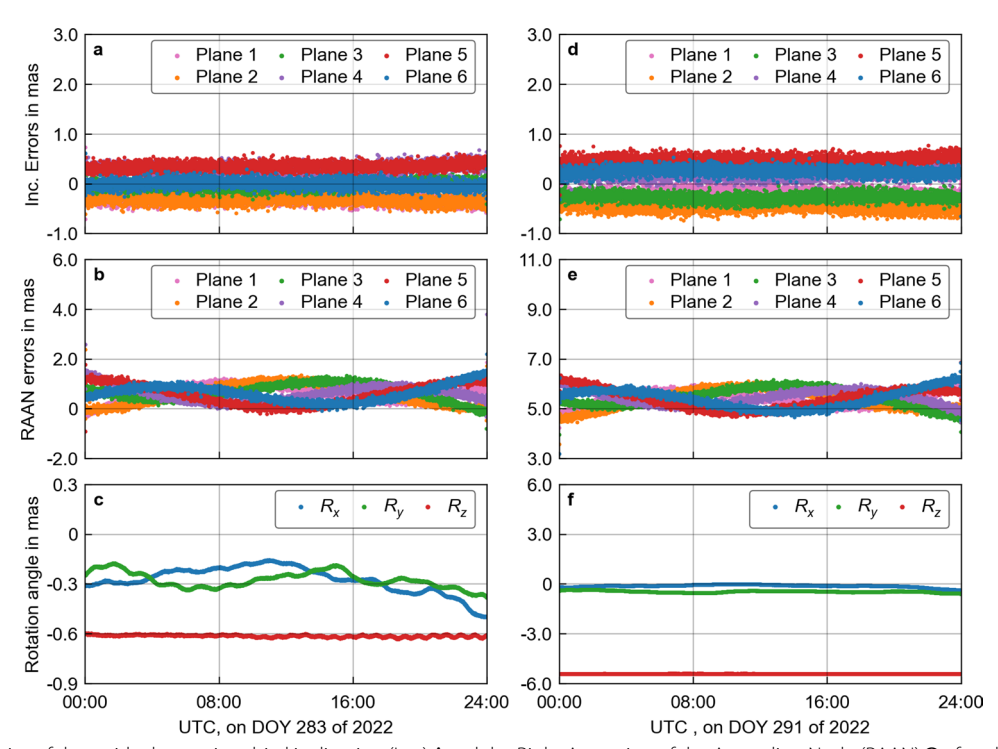


Fig. 9 Time series of the residual errors in orbital inclination (Inc.) i and the Right Ascension of the Ascending Node (RAAN)  $\Omega$  of each LEOs in every orbit plane as well as the residual constellation's rotation angles  $R_x$ ,  $R_y$  and  $R_z$  on DOY 283 a, b, c and 291 d, e, f of 2022 after rotation correction using broadcast ephemeris

Qin et al. Satellite Navigation (2025) 6:21 Page 12 of 21

**Table 4** The mean values and standard deviations of the residual errors of orbital inclination of each orbit plane of the LEO constellation

DOY	The residual errors of the orbital inclination in mas						
	Plane 1	Plane 2	Plane 3	Plane 4	Plane 5	Plane 6	
283	$(-31.5 \pm 8.4) \times 10^{-2}$	$(-32.2 \pm 8.3) \times 10^{-2}$	$(-1.6 \pm 8.3) \times 10^{-2}$	$(31.8 \pm 8.5) \times 10^{-2}$	$(35.1 \pm 7.8) \times 10^{-2}$	$(-0.3 \pm 8.2) \times 10^{-2}$	
291	$(1.6 \pm 8.4) \times 10^{-2}$	$(-2.0 \pm 8.1) \times 10^{-2}$	$(-0.6 \pm 8.4) \times 10^{-2}$	$(-1.0 \pm 8.3) \times 10^{-2}$	$(3.3 \pm 8.2) \times 10^{-2}$	$(-0.8 \pm 8.1) \times 10^{-2}$	

**Table 5** The mean values and standard deviations of the residual errors of the Right Ascension of the Ascending Node (RAAN) of each orbit plane of the LEO constellation

DOY	The residual errors of the RAAN in mas						
	Plane 1	Plane 2	Plane 3	Plane 4	Plane 5	Plane 6	
283	$(60.3 \pm 32.9) \times 10^{-2}$	$(57.2 \pm 41.2) \times 10^{-2}$	$(66.3 \pm 35.7) \times 10^{-2}$	$(62.4 \pm 32.0) \times 10^{-2}$	$(58.4 \pm 40.9) \times 10^{-2}$	$(63.0 \pm 33.6) \times 10^{-2}$	
291	$(1.4 \pm 27.8) \times 10^{-2}$	$(-4.6 \pm 38.5) \times 10^{-2}$	$(0.8 \pm 37.3) \times 10^{-2}$	$(2.0 \pm 28.6) \times 10^{-2}$	$(-0.8 \pm 39.9) \times 10^{-2}$	$(2.2 \pm 38.6) \times 10^{-2}$	

firstly compute the orbit errors of the BDS-3 broadcast ephemerides from DOY 277 to 291 and then determine the systematic errors contained in the broadcast ephemerides using Helmert transformation. Given the focus of this study on rotational effects, we specifically analyze the systematic rotation errors in the broadcast ephemerides. As illustrated in Fig. 10a-c, the along-track, crosstrack, and radial components of the broadcast ephemeris orbit errors range from 14.9 cm to 56.7 cm, 12.5 cm to 54.6 cm, and approximately 16.0 cm, respectively. Notably, during DOY 289 to 291, the along- and cross-track errors exhibit a significant increase, which coincides with the sharp rise in  $R_z$  as shown in Fig. 10 (d). According to Chen et al. (2021), predicted ERP are used in generating the BDS-3 broadcast ephemerides and the accumulated ERP prediction errors can cause a systematic overall shift of the BDCS implied in the broadcast ephemeris, introducing systematic errors into the broadcast ephemeris, including the systematic rotation errors. The pronounced orbit errors observed during DOY 289 to 291, as shown in Fig. 10a and b, may be partially attributed to the relatively large systematic rotation errors contained in the broadcast ephemerides, as indicated in Fig. 10d.

Using the determined rotation angles in the broadcast ephemeris, as shown in Fig. 10d, a rotation correction matrix is constructed, expressed like Eq. (6), to correct the systematic rotation errors in the broadcast ephemerides. The corrected orbits are then compared with the precise ephemerides, with a particular focus on the improvements of orbit errors in the along-track and cross-track directions during DOY 289 to 291, as illustrated in Fig. 11. The results show that, in the along-track direction, the orbit errors are reduced by 9.5 cm, 15.2 cm, and 19.1 cm, respectively. In the cross-track direction,

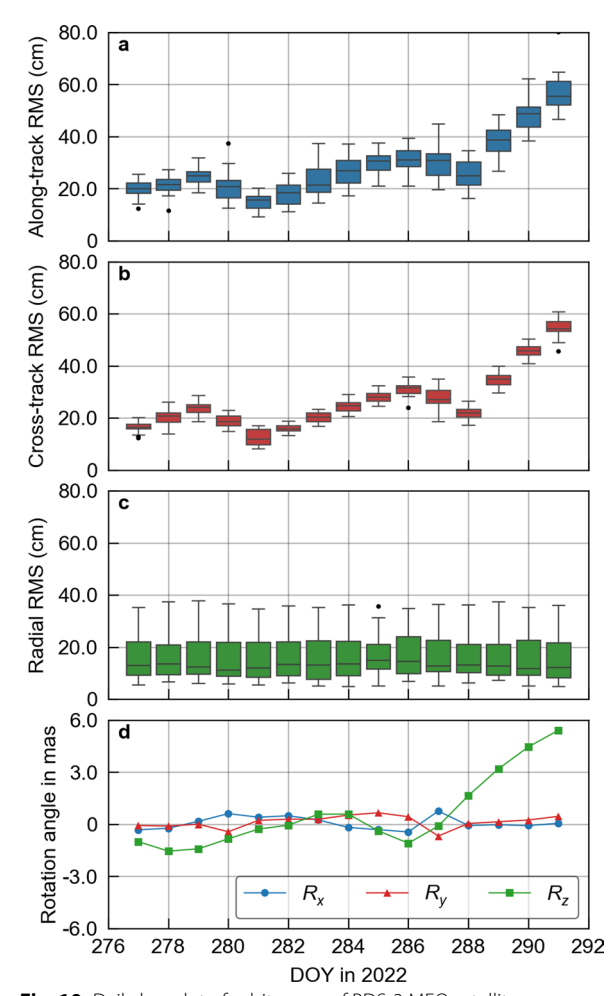


**Fig. 10** Daily boxplot of orbit errors of BDS-3 MEO satellites of the broadcast ephemerides in the along-track **a**, cross-track **b** and radial **c** directions, respectively. Subplot d represents the daily systmatic rotation errors of the BDCS realized by broadcast ephemerides with respect to that realized by precise ephemerides

Qin et al. Satellite Navigation (2025) 6:21 Page 13 of 21

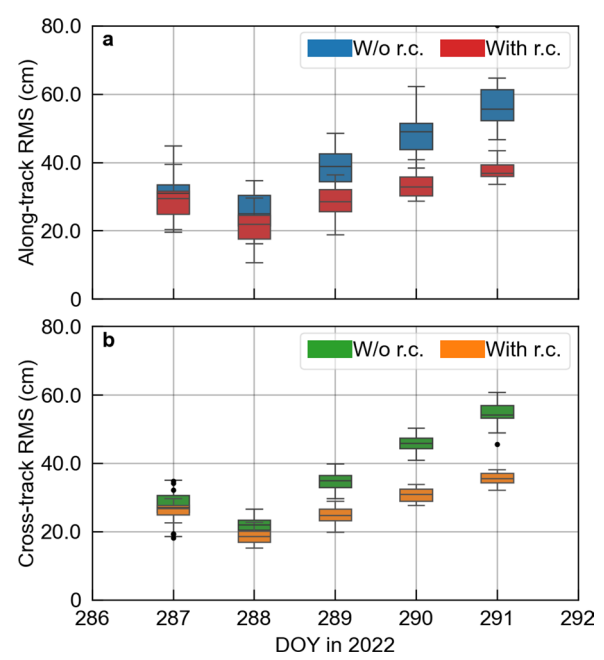


**Fig. 11** Daily boxplot of orbit errors of BDS-3 MEO satellites of the broadcast ephemerides in the along-track **a**, cross-track **b** without (W/o r.c.) or with (With r.c.) rotation correction

the corresponding improvements are 10.0, 15.2, and 19.1 cm. These findings demonstrate that systematic rotation errors in the broadcast ephemerides can introduce orbit deviations at the decimeter level. In contrast, when the broadcast ephemerides contain minimal rotation errors, the resulting orbit discrepancies are limited to the centimeter level. For example, on DOY 287 and 288, the improvements in along-track orbit errors are 1.2 and 4.0 cm, while the cross-track improvements are 1.0 cm and 3.0 cm, respectively.

Due to these systematic rotation errors in the broadcast ephemeris, some residual rotation errors remain in the rotation-corrected integrated POD solutions. As shown in Fig. 9f, residual rotation in  $R_z$  emerges, reaching nearly  $54.1 \times 10^{-1}$  mas, which is comparable to the systematic rotation errors in the broadcast ephemeris on DOY 291, as illustrated in Fig. 10d. This may be the reason for those

residual systematic errors in the RAAN  $\Omega$  whose magnitude is nearly the same as that of the residual rotation in  $R_z$ , as shown in Fig. 9e, which inevitably degrades the accuracy of the rotation-corrected integrated POD solutions. In comparison, the systematic errors in the broadcast ephemeris on DOY 283 are relatively small, as illustrated in Fig. 10d. After rotation correction, no evident residual rotation errors are presented as shown in Fig. 9c. Correspondingly, the residual errors in the orbital inclination and the RAAN reach only the sub-mas level, indicating that the systematic errors in both the orbital inclination i and the RAAN  $\Omega$  have been effectively corrected, ensuring accurate POD solutions.

Regarding orbit accuracy, Table 6 presents the constellation averaged RMS orbit errors in the along-track, cross-track, and radial directions for both the LEO constellation and BDS-3 MEOs, with and without rotation correction, over the entire POD processing period. The application of rotation correction can improve substantialy orbit accuracy is observed in both the along-track and cross-track directions across the unified constellation. The average RMS orbit error in the along-track direction for LEO satellites decreases from 22.7 to 1.3 cm, while that for BDS-3 MEOs are reduced from 124.3 to 13.2 cm. In the cross-track direction, the averaged RMS orbit error for LEOs is reduced from 39.3 to 4.2 cm, and for BDS-3 MEOs, from 137.8 to 13.7 cm. However, as discussed previously, the accuracy of the rotation-corrected POD solutions is affected by the residual rotation errors, which stem from the systematic rotation errors in the broadcast ephemerides.

To further assess the effectiveness of the rotation correction method in the situation of a more accurate spatial reference is available, the method is applied after eliminating the systematic rotation errors in the broadcast ephemeris. Table 7 summarizes the residual errors in orbital inclination i, RAAN  $\Omega$ , and the residual rotation angles of the coordinate system implied in the integrated POD solutions after the rotation correction with or without the influence of the systematic rotation errors in the broadcast ephemeris on DOY 291. When employing the

**Table 6** Constellation averaged RMSs of orbit errors of the integrated POD solutions with and without rotation correction (rot. cor.) using the rotation method in the along-track (A), cross-track (C) and radial (R) directions for the LEO constellation and BDS-3 MEOs over the entire POD process period

Rot. cor. application	RMSs of orb	oit errors (cm)				
	LEO constellation			BDS-3 MEOs		
	A	С	R	A	С	R
W/o rot. cor	22.7	39.3	0.2	124.3	137.8	3.4
With rot. cor	1.3	4.2	0.2	13.2	13.7	3.4

Qin *et al. Satellite Navigation (2025) 6:21* Page 14 of 21

**Table 7** LEO constellation mean and standard deviations of residual errors of the orbital inclination i and the RAAN  $\Omega$  after rotation correction using broadcast ephemeris with and without broadcast ephemeris systematic rotation errors influence (sys. rot. errors), as well as the residual constellation's rotation angles  $R_X$ ,  $R_V$  and  $R_Z$  on DOY 291, 2022

Sys. rot. errors	Residual errors of $i$ and $\Omega$ in $10^{-2}$ mas		Residual rotation angles in 10 <sup>-2</sup> mas		
	i	Ω	R <sub>x</sub>	$R_y$	Rz
With sys. rot. errors	0 ± 35.0	542.0 ± 35.0	$-12.0 \pm 8.0$	$-46.0 \pm 6.0$	$-542.0 \pm 1.0$
W/o sys. rot. errors	$0 \pm 12.0$	$0 \pm 36.0$	$2.0 \pm 8.0$	$-1.0 \pm 6.0$	$0 \pm 1.0$

precise spatial reference, the residual  $R_x$  and  $R_y$  further decreases from  $-12.0 \times 10^{-2}$  mas to  $-2.0 \times 10^{-2}$  mas, from  $-46.0 \times 10^{-2}$  mas to  $-1.0 \times 10^{-2}$  mas, respectively; for  $R_z$ , the residual of  $-542.0 \times 10^{-2}$  mas is nearly eliminates. Consequently, the systematic errors in the orbital inclination i are mostly eliminated. Additionally, the residual errors of approximately 5.0 mas in the RAAN  $\Omega$  are also effectively corrected, indicating that the overall rotation of the unified constellation are further corrected.

Figure 12 presents the daily constellation averaged RMS orbit errors of the unified constellation after rotation correction using BDS-3 broadcast ephemerides with and without systematic rotation errors as references, respectively. It is evident that applying the rotation correction using broadcast ephemerides free from systematic

rotation errors results in a significant reduction of orbit errors in both the along-track and cross-track directions for the BDS-3 MEOs and the LEO constellation. In the entire simulation period, the averaged RMS orbit errors of the LEO constellation decrease from 12.7 to 5.4 mm in the along-track direction and from 41.6 to 8.3 mm in the cross-track direction. For the BDS-3 MEOs, the errors are reduced from 132.0 mm and 136.7 mm to 21.7 mm and 21.6 mm, respectively.

These results demonstrate that the rotation correction method effectively mitigates the overall rotation of the constellation. They also indicate that, even when decimeter-level broadcast ephemerides are used during the POD processing, their stochastic errors have less impact on the estimation of systematic rotation angles. It is primarily

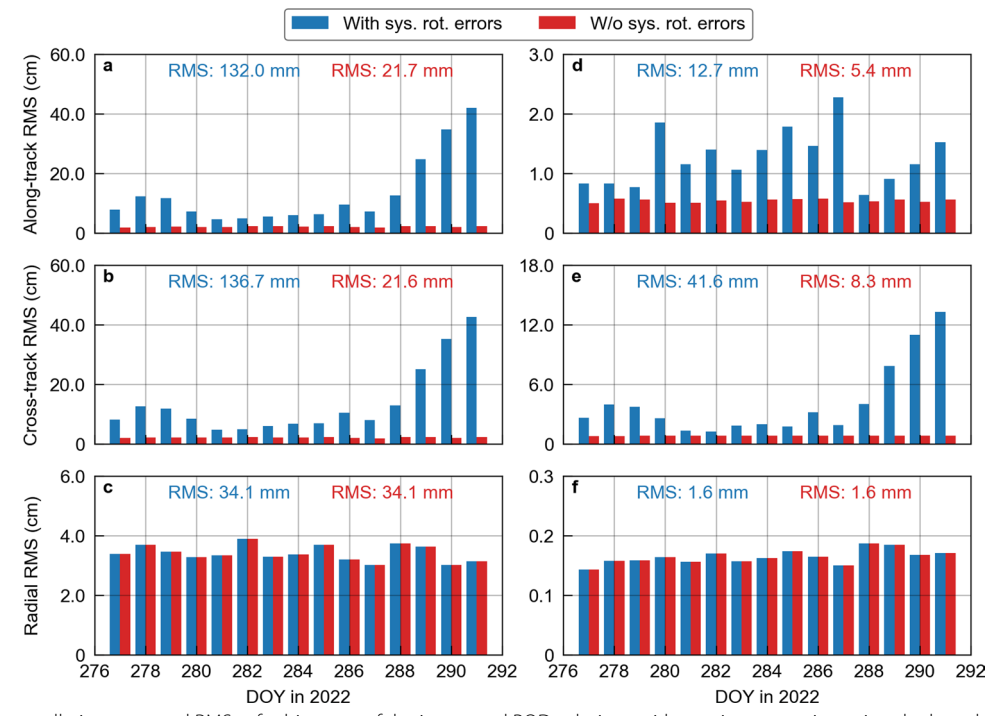


Fig. 12 Daily constellation averaged RMSs of orbit errors of the integrated POD solutions with rotation correction using the broadcast ephemerides with and without the broadcast ephemeris systematic rotation errors (sys. rot. errors) influence, respectively. a, b, c and d, e, f are statistics of the BDS-3 MEO satellites and the LEO constellation, respectively

Qin et al. Satellite Navigation (2025) 6:21 Page 15 of 21

the systematic rotational biases in the broadcast ephemerides that influence the estimated angles. Besides, the systematic rotation angles determined using the integrated POD solutions of BDS-3 MEO satellites can be used to effectively correct the systematic rotational errors in the LEO constellation. This reflects a strong connection established between the high and low constellation by using LEO satellites' onboard GNSS observations and integrated POD processing, which results in a consistent systematic rotation across the entire unified constellation, forming the foundation for the effectiveness of this rotation correction method.

#### Benefits of employing ISL

To evaluate the performance of the rotation correction method when only a subset of LEOs provides onboard BDS-3 observations, Strategy 2 is implemented. To avoid the impact of systematic rotation errors in the broadcast ephemeris, precise ephemerides are used as the reference for performing the rotation correction. Figure 13 presents the daily constellation averaged RMS orbit errors in the along-track, cross-track, and radial directions for the various scenarios where the number of LEO satellites supplying BDS-3 observations is different. The results demonstrate that even with only 36 LEOs providing onboard BDS-3 observations, this rotation correction

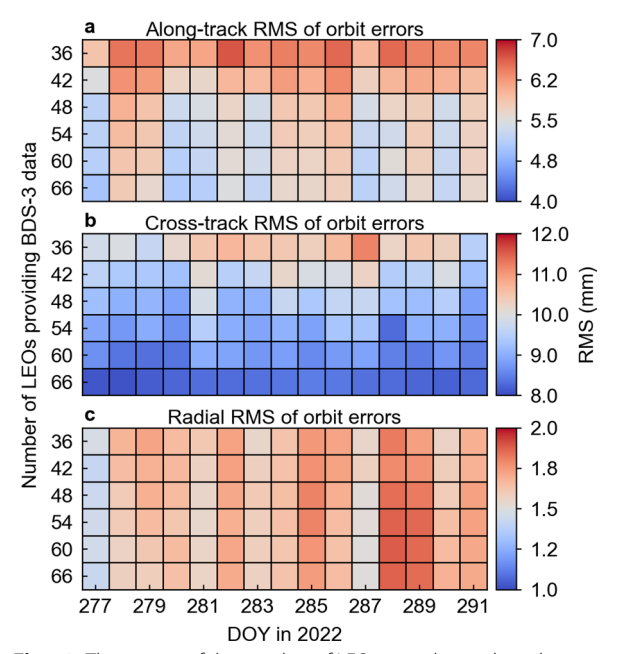


**Fig. 13** The impact of the number of LEOs providing onboard BDS-3 observations on the performance of the rotation correction method for the LEO constellation, using BDS-3 precise ephemeris as a reference. Each elemental square represents the daily constellation averaged RMS orbit errors in the along-track, cross-track, and radial components, respectively

method can also effectively mitigate the rotation in the integrated POD solutions, achieving orbit accuracy comparable to that of Strategy 1 after rotation correction. As the number of LEOs providing BDS-3 observations increases, the accuracy of the rotation-corrected integrated POD solutions improves accordingly. However, once the number approaches 48, further improvements become marginal. This benefit arises from the ISL connectivity among LEOs. A subset of LEOs providing BDS-3 observations can, together with all BDS-3 MEOs, form an initial high-low unified constellation. Through ISL, the remaining LEOs without BDS-3 observations can link to this core group, thereby establishing a fully unified constellation encompassing all LEOs and BDS-3 MEOs. Leveraging this feature in orbit determination operations allows a reduction in the volume of onboard BDS-3 data that must be processed, thereby alleviating computational demands to some extent.

As previously discussed, the accuracy of the rotationcorrected POD solutions improves with the increasing number of LEO satellites providing onboard BDS-3 observations. This can be attributed to the limited tracking data as well as the poor observation geometry between BDS-3 MEOs and a small subset of LEOs when fewer LEOs supply BDS-3 observations. In such conditions, it becomes difficult to accurately determine the relative positions between the BDS-3 MEOs and these LEOs. As a result, even when using precise ephemerides as references, the estimated rotation angles may not faithfully reflect the actual rotation of the unified constellation, thereby reducing the effectiveness of the correction. As the number of LEOs providing BDS-3 observations increases, the quantity and geometry of the tracking data improve significantly. This facilitates a more accurate determination of the relative positions between the BDS-3 MEOs and the observing LEOs, yielding more reliable estimates of the constellation rotation angles. Subsequently, through the ISL that connects all LEO satellites, these refined rotation parameters can be employed across the entire constellation. Consequently, high-precision, rotation-corrected orbits for the full unified constellation can be achieved.

# **Rotation correction with predicted ERP**

In the certain POD operational scenarios where observed ERP is unavailable, predicted ERP is used in both the integrated POD and the rotation correction processing of the rotation correction method. In this subsection, the predicted ERP from IERS Bulletin A is utilized to assess the influence of the predicted ERP on this method's performance. Figure 14 presents the differences between the predicted and observed ERPs in the entire POD period. The dashed lines indicate the update days of the predicted

Qin et al. Satellite Navigation (2025) 6:21 Page 16 of 21

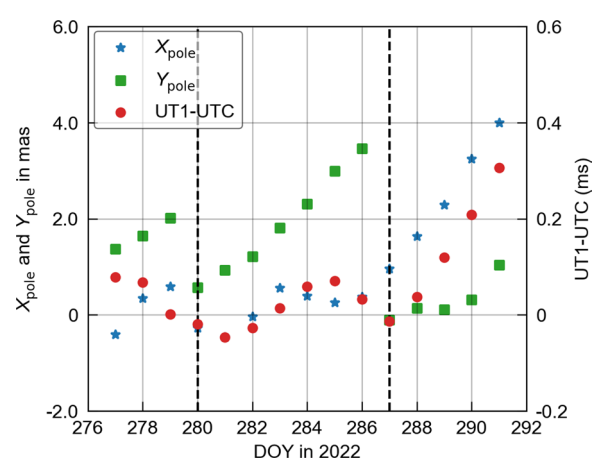


**Fig. 14** Daily prediction errors of Earth Rotation Parameters (ERP) obtained from IERS Bulletin A with respective to the observed ERP from IERS Bulletin B

**Table 8** Summary of the usage strategies using Earth Rotation Parameters (ERP) in the integrated POD processing and transformation of BDS-3 broadcast ephemeris from ECEF to ECI as well as the strategies using the reference BDS-3 broadcast ephemeris (Ref. broadcast ephemeris) in roation correction process

Case ID	ERP usage strategies		Ref. broadcast ephemeris
	Integrated POD	ECEF to ECI	
Case 1	P-ERP	O-ERP	Without systematic rotation errors
Case 2		P-ERP	Without systematic rotation errors
Case 3		O-ERP	With systematic rotation errors
Case 4		P-ERP	With systematic rotation errors

ERPs, with a 7-day update cycle adopted in this study (Chen et al., 2021; Xia et al., 2024). It is evident that the prediction errors for  $X_{\rm pole}$ , and  $Y_{\rm pole}$ , and UT1-UTC are minimal on the update days and gradually increase until the next update. In the entire POD processing period, the maximum deviations reached 3.9 mas for  $X_{\rm pole}$ , 3.5 mas for  $Y_{\rm pole}$ , and 0.3 ms for UT1-UTC. The 0.3 ms UT1-UTC error corresponds to approximately 4.5 mas in Greenwich Apparent Sidereal Time (GAST), which affects the Earth's rotational angle. This GAST deviation, combined with forecast errors in  $X_{\rm pole}$ , and  $Y_{\rm pole}$ , will introduce systematic rotation errors into the POD results, predominantly degrading the along-track and cross-track orbit accuracy (Xia et al., 2024).

To comprehensively evaluate the impact of the predicted ERP errors on the performance of the rotation correction method, four ERP employment strategies are designed, as summarized in Table 8. In all cases, the integrated POD is conducted using the predicted ERP. In case 1, observed ERP and BDS-3 broadcast ephemerides without systematic rotation errors are employed in the rotation correction step. Without any systematic errors, this configuration is intended to demonstrate the influence of the predicted ERP errors on the integrated POD process. In cases 2, 3, and 4, the effects of using either Observed ERP (O-ERP) or Predicted ERP (P-ERP) along with the BDS-3 broadcast ephemerides with or without eliminating systematic rotation errors in the rotation correction step are analyzed. Among these cases, only case 2 and case 4 are representative of practical operational scenarios. Cases 1 and 3 serve as auxiliary configurations to help illustrate and interpret the roles of ERP errors in the rotation correction framework.

Figure 15 illustrates the daily constellation averaged RMS orbit errors of the LEO constellation in the alongtrack and cross-track directions for cases 1 to 4, while the corresponding averaged RMS errors in the entire POD period are summarized in Table 9. In case 1, the integrated POD is performed using predicted P-ERP, while rotation correction is applied using observed O-ERP and BDS-3 broadcast ephemeris that do not contain systematic rotation errors. In this configuration, the alongtrack and cross-track RMS errors are 6.0 mm and 8.6 mm, respectively. These results are consistent with those shown in Fig. 12d and e with orbit errors of 5.4 mm and 8.3 mm, respectively. This consistency indicates that, in the rotation correction method, the use of P-ERP in the integrated POD processing introduces only a limited impact on the final corrected solutions. The errors caused by P-ERP in the integrated POD processing are likely absorbed into the integrated POD results as systematic constellation-wide rotation errors. Then in the rotation angles determination as illustrated in Fig. 3, when broadcast ephemeris without systematic rotation errors is transformed from ECEF to ECI using O-ERP, an accurate spatial reference free of any systematic rotation interference can be obtained. Then applying this reference in the rotation correction step, the rotation errors in the integrated POD solutions can be effectively eliminated, yielding excellent rotation corrected POD solutions.

In case 2, the constellation's rotation correction is performed using P-ERP and broadcast ephemerides that are free from systematic rotation errors. As shown in Fig. 15, compared to case 1, the orbit accuracy in case 2 deteriorates in both the along-track and the cross-track directions, with RMS values increasing to 8.2 mm and 34.8 mm, respectively. Figure 16a presents the residual rotation angles of the LEO constellation after rotation correction in case 2. It is observed that the residual rotations around the *x*- and *y*-axes

Qin et al. Satellite Navigation (2025) 6:21 Page 17 of 21

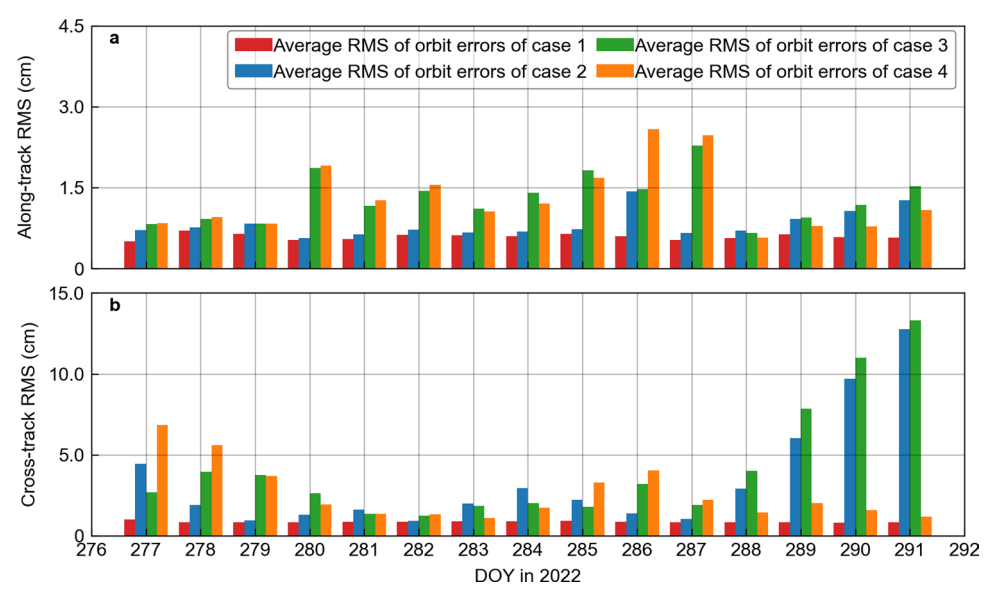


**Fig. 15** Daily constellation averaged RMSs of orbit errors in the along-track and cross-track directions of the rotation corected integrated POD solutions of the LEO constellation derived from the cases 1, 2, 3 and 4, respectively

**Table 9** Mean of daily constellation averaged RMS of orbit errors in the along-track, cross-track and radial directions of the rotation corrected integrated POD solutions of the LEO constellation in the entire POD process period derived for the cases 1, 2, 3 and 4, respectively

CASE ID	RMS of orbit errors (mm)				
	A	С	R		
Case 1	6.0	8.6	1.6		
Case 2	8.2	34.8	1.6		
Case 3	13.0	41.7	1.6		
Case 4	13.1	26.2	1.6		

are generally small, except for a noticeable deviation around the y-axis on DOY 286, which corresponds to the large orbit errors in the along-track on the same day. In contrast, more pronounced residual rotations are seen around the z-axis, exhibiting temporal variations that closely align with the cross-track orbit errors. In case 2, in the rotation angle determination step, the broadcast ephemeris free from systematic rotation errors is transformed from ECEF to ECI using P-ERP. The prediction errors in the P-ERP can introduce systematic rotation errors into the resulting spatial reference implied in the transformed broadcast ephemeris. Consequently, when the biased spatial reference is used for rotation correction, the systematic rotation errors are retained in the corrected integrated POD solutions, thereby degrading their accuracy. This explains the residual y-axis rotation error on DOY 286, which

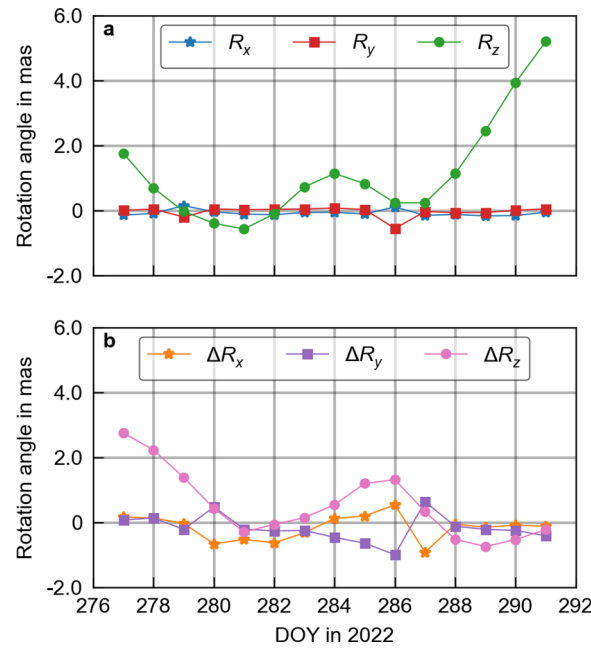


**Fig. 16** Daily residual constellation's rotation angles  $R_x$ ,  $R_y$  and  $R_z$  of case 2 **a**; The daily rotation angles difference between the residual constellation's rotation angles derived from the case 2 and the daily systematic rotation errors contained in the BDS-3 broadcast ephemerides

aligns with a significant prediction error in the  $Y_{\rm pole}$  component, and the prominent z-axis residuals from DOY 287 to 291, which correspond to the variations in the UT1-UTC prediction errors, as shown in Fig. 14.

Qin et al. Satellite Navigation (2025) 6:21 Page 18 of 21

Overall, these results demonstrate that when broadcast ephemerides free of systematic rotation errors are used for rotation correction, predicted ERP can introduce systematic rotation errors into the corrected POD solutions, ultimately reducing their accuracy.

In case 3, rotation correction for the LEO constellation is performed using O-ERP and broadcast ephemerides that contain systematic rotation errors. As previously discussed, the impact of using predicted ERP in the integrated POD processing on the final rotation-corrected POD solutions is relatively limited. When observed ERP is employed in the rotation angle determination, the systematic rotation errors inherent in the broadcast ephemeris remain in the spatial reference frame realized by the transformed broadcast ephemeris. Then applying this spatial reference for rotation correction, this remained systematic rotation errors can degrade the rotationcorrected integrated POD solutions. The degraded POD solutions are consistent with the results presented in Sect. 4.2, where rotation correction is conducted using broadcast ephemerides having systematic rotation errors. The RMS orbit errors in the along-track and crosstrack directions in case 3 increase to 13.0 mm and 41.7 mm, respectively, closely matching the values shown in Fig. 12d and e. Furthermore, the daily variations in the cross-track errors as shown in Fig. 14 exhibit a strong correlation with the temporal evolution of the z-axis systematic rotation errors in the BDS-3 broadcast ephemerides, as illustrated in Fig. 10d.

In case 4, which is the most representative of practical POD scenarios where only predicted ERP are available, both the predicted ERP errors and the systematic rotation errors in the broadcast ephemerides are present in the rotation correction. In the generation of broadcast ephemerides, predicted ERP are used to transform POD orbits from the ECI to the ECEF, thereby introducing ERP prediction errors into the broadcast ephemeris presented in the ECEF. When these ephemerides are used for rotation angle determination as shown in Fig. 3, the same or similar predicted ERP are again employed to transform them back from ECEF to ECI. This round-trip transformation can partially cancel out the systematic rotation errors contained in the broadcast ephemerides, resulting in a relatively accurate spatial reference for rotation correction. As a result, orbit accuracy in case 4 is improved compared to case 3, with RMS errors reduced to 13.1 mm in the along-track and 26.2 mm in the crosstrack directions. To illustrate this effect, we calculate the angle differences,  $\Delta R_x$ ,  $\Delta R_y$ , and  $\Delta R_z$ , between the residual rotation angles in the rotation corrected POD solutions using predicted ERP as shown in Fig. 16a and the systematic rotation errors in the broadcast ephemerides exhibited in Fig. 10d and show them in Fig. 16b. On DOY

277 and 278,  $\Delta R_z$  reaches approximately 2.0 mas, corresponding to the elevated cross-track errors observed in Fig. 15 for case 4. From DOY 279 to 287, the variations in  $\Delta R_x$ ,  $\Delta R_y$ , and  $\Delta R_z$  contribute to orbit errors mainly in the along-track direction. From DOY 288 to 291, the systematic rotation errors in all three axes are largely mitigated by the use of predicted ERP, resulting in reduced orbit errors. Overall, the use of predicted ERP in the rotation angle determination process can partially compensate for the systematic rotation errors present in the broadcast ephemerides, enabling the construction of a relatively accurate spatial reference for rotation correction. It is expected that, as the update frequency and prediction accuracy of ERP used in generating BDS-3 broadcast ephemerides continue to improve, the performance of the rotation correction method, using daily observed or timely updated predicted ERP, will asymptotically approach that of case 1.

#### Conclusion

This paper introduces a rotation correction method for LEO constellations, enabling the generation of lowlatency and high-accuracy orbit solutions while reducing the needs for dedicated ground stations to track the LEO constellation. This is achieved with an integrated POD process that uses ISL ranging measurements and onboard BDS-3 observations from LEOs, while simultaneously estimating the orbits of the unified constellation consisting of both LEO and 24 BDS-3 MEOs. Due to the lack of absolute spatial reference, the integrated POD solutions inevitably subject to a common systematic rotation. To correct this rotation, the BDCS realized by the readily available broadcast ephemeris is employed to be treated as the spatial reference and utilized to determine the systematic rotation angles  $R_x$ ,  $R_y$ , and  $R_z$  of the coordinate system implied in the integrated POD solutions. Then a rotation correction matrix is formed by the three rotation angles to correct the systematic rotation errors that arise in the integrated POD solutions. To validate the feasibility and effectiveness of this approach, a LEO constellation consisting of 66 satellites is simulated, along with ISL and onboard BDS-3 observations. Besides, two POD strategies are set up for validation and analysis.

In Strategy 1, the performance of the proposed rotation correction method is examined. The high-low unified constellation initially exhibits overall rotation after integrated POD processing due to the absence of a spatial reference. After applying the rotation correction method using the BDCS realized by broadcast ephemerides, the RMS orbit errors in the along-track and cross-track directions are reduced respectively from 124.3 cm and 137.8 cm to 13.2 cm and 13.7 cm for BDS-3 MEOs, and from 22.7 and 39.3 cm to 1.3 and 4.2 cm for the LEOs.

Qin et al. Satellite Navigation (2025) 6:21 Page 19 of 21

It demonstrates that the overall rotation of the unified constellation is effectively corrected. However, due to systematic rotation errors inherent in the BDS-3 broadcast ephemeris, some residual rotation errors remain in these corrected POD solutions. After excluding these systematic rotation errors contained in the broadcast ephemeris, the RMS orbit errors in the along-track and cross-track components are further reduced to 0.5 and 0.8 cm for the LEOs, and to 2.2 and 2.2 m for BDS-3 MEOs. These results demonstrate that the rotation correction method is feasible and effective in correcting the constellation's overall rotation. Since the constellation's overall rotation has a limited impact on the precision of the integrated POD solutions in the radial direction, the radial orbit errors for both LEOs and BDS-3 MEOs remain consistent at 0.2 cm and 3.4 cm, respectively, regardless of whether the rotation correction is applied.

In Strategy 2, we explore the performance of the rotation correction method when only a subset of LEO satellites provides onboard BDS-3 data. The results indicate that when the amount of onboard BDS-3 observations from these LEOs is sufficient to accurately determine the relative positions of the BDS-3 MEOs and these LEOs, the connection of all LEOs via ISL can accurately determine the orbits of all LEOs and BDS-3 MEOs with the rotation correction method.

When observed ERP are unavailable for this rotation correction method, we finally assess the impact of predicted ERP on the performance of this method. The analysis indicates that ERP prediction errors introduced in the integrated POD process may propagate into the integrated POD results as systematic rotation errors. These errors can be effectively mitigated using the rotation correction method. However, in the rotation correction process, ERP prediction errors can degrade the rotation corrected POD results. Particularly, when the BDS-3 broadcast ephemeris does not contain systematic rotation errors, the ERP prediction errors introduced in the broadcast ephemeris transformation from the ECEF to ECI can degrade the rotation-corrected POD accuracy from 0.6 cm, 0.9 cm, and 0.2 cm to 0.8 cm, 3.5 cm, and 0.2 cm in the along-track, cross-track, and radial directions, respectively. When the broadcast ephemeris contains systematic rotation errors originating from its generation process, the ERP prediction errors can partially offset these systematic rotation errors. As a result, the rotation-corrected POD accuracy improves, achieving 1.3 cm, 2.6 cm, and 0.2 cm in the along-track, crosstrack, and radial directions, respectively. It is expected that, as the update frequency and prediction accuracy of the ERP used in generating BDS-3 broadcast ephemerides continue to improve, the performance of the introduced constellation's rotation correction method, using daily observed or timely updated predicted ERP, will obtain excellent POD solutions.

The analysis indicates that unlike general POD processing approaches that fix GNSS satellite orbits for obtaining spatial reference, benefiting from the integrated estimation of the orbits of LEO and GNSS satellites, this method can mitigate the degradation of POD accuracy caused by large broadcast ephemeris errors, meanwhile it can extract the relatively accurate BDCS implied in the readily available broadcast ephemeris for rotation correction, achieving the high-precision and low-latency LEO constellation's POD. Moreover, by acquiring the external spatial reference from the established BDCS for the LEO constellation, this method can significantly reduce the dependence of the LEO constellation on the ground tracking stations, thereby lowering construction and maintenance costs.

This paper primarily focuses on the performance of the proposed rotation correction method. Further validation of its performance with other navigation systems, e.g., GPS and Galileo, and even multi-system is necessary. Besides, the impact of the translation and scale factors on the relationship between the coordinate systems needs further study. Additionally, more systematic errors should be incorporated into the observation simulations, which are more representative of real-world conditions. The impact of errors in the dynamic models of both LEOs and BDS-3 MEOs also requires examination to analyze the relationship between the overall rotation and these introduced errors. Finally, exploring the relationship between the number and distribution of LEO satellites providing onboard BDS-3 observations and the effectiveness of the rotation correction method is an interesting topic for future research.

# Acknowledgements

We would like to thank the editors and reviewers for their valuable comments, which will significantly improve the quality of the manuscript. We are also grateful to IGS for providing the broadcast navigation files, and to GFZ for providing GNSS precise products.

#### **Author contributions**

L.M. proposed the initial idea of this work; Q.G.E. and X.X. developed the software; Q.G.E designed the experiment, carried out the simulations and drafted the article. J.K.C. and L.M. assisted in paper writing and revision. All authors read and approved the final manuscript.

# **Funding**

This study is financially supported by the National Natural Science Foundation of China (Grant Nos. 42204020, 42030109), and the China Postdoctoral Science Foundation (Grant Nos. 2021M702507).

#### Availability of data and materials

The datasets used and analyzed during this study are available from the corresponding author on reasonable request.

Qin et al. Satellite Navigation (2025) 6:21 Page 20 of 21

#### **Declarations**

#### **Competing interests**

Qile Zhao is an editorial board member for Satellite Navigation and was not involved in the editorial review or decision to publish this article. All authors declare that they have no competing interests.

#### **Author details**

<sup>1</sup>GNSS Research Center, Wuhan University, 129 Luoyu Road, Wuhan 430079, China. <sup>2</sup>Chongqing Satellite Network System Co., Ltd, Chongqing 401135, China. <sup>3</sup>Department of Land Surveying and Geo-Informatics, The Hong Kong Polytechnic University, Hong Kong 999077, China.

# Received: 11 November 2024 Revised: 30 June 2025 Accepted: 1 July 2025

Published online: 04 August 2025

#### References

- Ananda, M.P., Bernstein, H., Cunningham, K.E., Feess, W.A., & Stroud, E.G. (1990). Global Positioning System (GPS) autonomous navigation. In: IEEE Symposium on Position Location and Navigation. A Decade of Excellence in the Navigation Sciences, pp. 497–508.
- Arnold, D., Montenbruck, O., Hackel, S., & Sośnica, K. (2019). Satellite laser ranging to low earth orbiters: Orbit and network validation. *Journal of Geodesy*, 93(11), 2315–2334. https://doi.org/10.1007/s00190-018-1140-4
- Boucher, C., & Altamimi, Z. (2001). ITRS, PZ-90 and WGS 84: Current realizations and the related transformation parameters. *Journal of Geodesy, 75*(11), 613–619. https://doi.org/10.1007/s001900100208
- Bruinsma, S. (2015). The DTM-2013 thermosphere model. *Journal of Space Weather and Space Climate*, 5, A1. https://doi.org/10.1051/swsc/2015001
- Chen, G., Wei, N., Li, M., Zhao, Q., Niu, Y., Cai, H., & Meng, Y. (2021). Assessment of BDS-3 terrestrial reference frame realized by broadcast ephemeris: comparison with GPS/Galileo. *GPS Solutions*, 26(18), 1–16. https://doi.org/10.1007/s10291-021-01204-0
- Cheng, J., Liu, W., Zhang, X., Wang, F., Li, Z., Tang, C., Pan, J., & Chang, Z. (2023).

  On-board validation of BDS-3 autonomous navigation using inter-satellite link observations. *Journal Geodesy*, 97, 71. https://doi.org/10.1007/s00190-023-01759-5
- Dick, W. R., & Richter, B. (2004). The international earth rotation and reference systems service (IERS). In A. Heck (Ed.), *In: Organizations and strategies in astronomy. Astrophysics and space science library.* Springer.
- Fernández, F. A. (2011). Inter-satellite ranging and inter-satellite communication links for enhancing GNSS satellite broadcast navigation data. *Advances in Space Research*, 47(5), 786–801. https://doi.org/10.1016/j.asr. 2010.10.002
- Giorgi, G., Schmidt, T. D., Trainotti, C., Mata-Calvo, R., Fuchs, C., Hoque, M. M., Berdermann, J., Furthner, J., Günther, C., Schuldt, T., Sanjuan, J., Gohlke, M., Oswald, M., Braxmaier, C., Kalidakis, K., Dick, G., Flechtner, F., Ge, M., Glaser, S., ... Schuh, H. (2019). Advanced technologies for satellite navigation and geodesy. *Advances in Space Research*, 64(6), 1256–1273. https://doi. org/10.1016/j.asr.2019.06.010
- Günther, C. (2018). Kepler Satellite Navigation without Clocks and Ground Infrastructure (pp. 849–856). Florida.
- Guo, J. (2014). The impact of attitude, solar radiation and function model on precise orbit determination for GNSS satellite. Wuhan University.
- Guo, L., Wang, F., Gong, X., Sang, J., Liu, W., & Zhang, W. (2020). Initial results of distributed autonomous orbit determination for Beidou BDS-3 satellites based on inter-satellite link measurements. GPS Solutions, 24(3), 72. https://doi.org/10.1007/s10291-020-00985-0
- Hackel, S., Montenbruck, O., Steigenberger, P., Balss, U., Gisinger, C., & Eineder, M. (2017). Model improvements and validation of TerraSAR-X precise orbit determination. *Journal of Geodesy*, 91(5), 547–562. https://doi.org/10.1007/s00190-016-0982-x
- He, X., Hugentobler, U., Schlicht, A., Nie, Y., & Duan, B. (2022). Precise orbit determination for a large LEO constellation with inter-satellite links and the measurements from different ground networks: A simulation study. *Satellite Navigation*, 3(1), 22. https://doi.org/10.1186/s43020-022-00083-1

- Homssi, B., Al-Houranl, A., Wang, K., Conder, P., Kandeepan, S., Chol, J., Allen, B., & Moores, B. (2022). Next generation mega satellite networks for access equality: Opportunities, challenges, and performance. *IEEE Communications Magazine*, 60(4), 18–24. https://doi.org/10.1109/MCOM.001.2100802
- Hong, J.-H., Park, W., & Ryoo, C.-K. (2021). An autonomous space navigation system using image sensors. *International Journal of Control, Automation and Systems*, 19(6), 2122–2133. https://doi.org/10.1007/s12555-020-0319-7
- Jiang, K., Li, W., Li, M., Geng, J., Lyu, H., Zhao, Q., & Liu, J. (2023). Precise orbit determination of Haiyang-2D using onboard BDS-3 B1C/B2a observations with ambiguity resolution. *Satellite Navigation*, *4*(1), 28. https://doi.org/10.1186/s43020-023-00118-1
- Kur, T., & Kalarus, M. (2021). Simulation of Inter-Satellite Link schemes for use in precise orbit determination and clock estimation. Advances in Space Research, 68(12), 4734–4752. https://doi.org/10.1016/j.asr.2021.05.011
- Li, M., Huang, T., Li, W., & Zhao, Q. (2024). Overview of low earth orbit (LEO) navigation augmentation technology. *Journal of Geomatics*, 49(1), 20230484. https://doi.org/10.14188/j.2095-6045.20230484
- Li, M., Qin, G., Jiang, K., Wang, Y., & Zhao, Q. (2023a). Performance assessment of real-time orbit determination for the Haiyang-2D using onboard BDS-3/GPS observations. *Advances in Space Research*, 71(3), 1657–1669. https://doi.org/10.1016/j.asr.2022.09.050
- Li, M., Wang, Y., Li, W., Jiang, K., Zhang, Y., Lyu, H., & Zhao, Q. (2023b). Performance evaluation of real-time orbit determination for LUTAN-01B satellite using broadcast earth orientation parameters and multi-GNSS combination. *GPS Solutions*, 28(1), 52. https://doi.org/10.1007/s10291-023-01593-4
- Li, M., Zhang, J., Chen, G., Chen, L., & Zhao, Q. (2023c). Study on systematic errors of BDS-3 broadcast ephemeris and their effects with Helmert transformation. *Satellite Navigation*, *4*(1), 16. https://doi.org/10.1186/s43020-023-00107-4
- Li, X., Jiang, Z., Ma, F., Lv, H., Yuan, Y., & Li, X. (2019). LEO precise orbit determination with inter-satellite links. *Remote Sensing*, *11*(18), 2117. https://doi.org/10.3390/rs11182117
- Liu, L., Xu, J., Zhou, S., & Wu, F. (2019). Update on the BeiDou coordinate system (BDCS). In: Fourteenth Meeting of the International Committee on GNSS, ICG-14, 8–13, Bangalore, India, December 2019, UNOOSA https://www.unoosa.org/documents/pdf/icg/ 2019/icg14/WGD/icg14\_wgd\_01.pdf
- Liu, J., & Ge, M. (2003). PANDA software and its preliminary result of positioning and orbit determination. *Wuhan University Journal of Natural Sciences*, 8, 603–609. https://doi.org/10.1007/BF02899825
- Liu, W. (2008). Research and Simulation on Autonomous Orbit Determination and Combined Orbit Determination of Navigation Satellites. Wuhan University.
- Lv, Y., Geng, T., Zhao, Q., Xie, X., Zhang, F., & Wang, X. (2020). Evaluation of BDS-3 orbit determination strategies using ground-tracking and inter-satellite link observation. *Remote Sensing*, 12(16), 2647. https://doi.org/10.3390/rs12162647
- Lyard, F., Lefevre, F., Letellier, T., & Francis, O. (2006). Modelling the global ocean tides: Modern insights from FES2004. *Ocean Dynamics*, *56*(5–6), 394–415. https://doi.org/10.1007/s10236-006-0086-x
- Maine, K.P., Anderson, P., & Langer, J. (2003). Crossfinks for the next-generation gps. In: 2003 IEEE Aerospace Conference Proceedings (Cat. No.03TH8652). IEEE, Big Sky, Montana, USA, pp. 4\_1589-4\_1596
- Marshall, J. A., & Luthcke, S. B. (1994). Modeling radiation forces acting on Topex/Poseidon for precision orbit determination. *Journal of Spacecraft Rockets*, 31(1), 99–105. https://doi.org/10.2514/3.26408
- Marz, S., Schlicht, A., & Hugentobler, U. (2021). Galileo precise orbit determination with optical two-way links (OTWL): A continuous wave laser ranging and time transfer concept. *Journal of Geodesy*, *95*(85), 85. https://doi.org/10.1007/s00190-021-01534-4
- Menn, M.D., & Bernstein, H. (1994). Ephemeris observability issues in the Global Positioning System (GPS) autonomous navigation (AUTONAV). In: Proceedings of 1994 IEEE Position, Location and Navigation Symposium PLANS'94. IEEE, Las Vegas, NV, USA, pp. 677–680.
- Michalak, G., Glaser, S., Neumayer, K. H., & König, R. (2021). Precise orbit and Earth parameter determination supported by LEO satellites, inter-satellite links and synchronized clocks of a future GNSS. *Advances in Space Research*, 68(12), 4753–4782. https://doi.org/10.1016/j.asr.2021.03.008
- Montenbruck, O., Hackel, S., & Jäggi, A. (2018). Precise orbit determination of the Sentinel-3A altimetry satellite using ambiguity-fixed GPS carrier phase observations. *Journal of Geodesy*, *92*(7), 711–726. https://doi.org/10.1007/s00190-017-1090-2

Qin et al. Satellite Navigation (2025) 6:21 Page 21 of 21

- Montenbruck, O., Hackel, S., Wermuth, M., & Zangerl, F. (2021). Sentinel-6A precise orbit determination using a combined GPS/Galileo receiver. *Journal of Geodesy*, 95, 109. https://doi.org/10.1007/s00190-021-01563-z
- Montenbruck, O., Kunzi, F., & Hauschild, A. (2022). Performance assessment of GNSS-based real-time navigation for the Sentinel-6 spacecraft. GPS Solutions, 26, 12. https://doi.org/10.1007/s10291-021-01198-9
- Montenbruck, O., & Ramos-Bosch, P. (2008). Precision real-time navigation of LEO satellites using global positioning system measurements. *GPS Solutions*, 12(3), 187–198. https://doi.org/10.1007/s10291-007-0080-x
- Nicolini, L., & Caporali, A. (2018). Investigation on reference frames and time systems in multi-GNSS. *Remote Sensing*, 10(1), 80. https://doi.org/10.3390/ rs10010080
- Petit, G., & Luzum, B. (2010). IERS conventions (2010). Bureau International des Poids et mesures sevres (france),
- Rajan, J.A. (2002). Highlights of GPS II-R Autonomous Navigation. th Annual Meeting
- Rajan, J.A., Orr, M., & Wang, P. (2003b). On-orbit validation of GPS IIR autonomous navigation. In: Proceedings of ION AM 2003a, Institute of Navigation, Albuquerque, NM, USA, June 23–25, pp. 411–419.
- Rajan, J.A., Brodie, P., & Rawicz, H. (2003a). Modernizing GPS autonomous navigation with anchor capability. In: Proceedings of ION GPS/GNSS 2003b, Portland, Oregon, September 2003b, pp. 1534–1542.
- Reid, T. G., Neish, A. M., Walter, T. F., & Enge, P. K. (2016). *Leveraging Commercial Broadband LEO Constellations for Navigating* (pp. 2300–2314). Portland.
- Ren, X., Yang, Y., Zhu, J., & Xu, T. (2017). Orbit determination of the Next-Generation Beidou satellites with Intersatellite link measurements and a priori orbit constraints. Advances in Space Research, 60(10), 2155–2165. https://doi.org/10.1016/j.asr.2017.08.024
- Schlicht, A., Marz, S., Stetter, M., Hugentobler, U., & Schäfer, W. (2020). Galileo POD using optical inter-satellite links: A simulation study. *Advances in Space Research*, 66(7), 1558–1570. https://doi.org/10.1016/j.asr.2020.06.
- Shako, R., Förste, C., Abrikosov, O., Bruinsma, S., Marty, J., Lemoine, J., Flechtner, F., Neumayer, H., & Dahle, C. (2014). EIGEN-6C: a high-resolution global gravity combination model including GOCE data. In F. Flechtner, N. Sneeuw, & W.-D. Schuh (Eds.), Observation of the system earth from space CHAMP, GRACE, GOCE and future missions Advanced Technologies in Earth Sciences (pp. 155–161). Springer.
- Shang, L., Chang, J., Zhang, J., & Li, G. (2018). Precision analysis of autonomous orbit determination using star sensor for Beidou MEO satellite. *Advances in Space Research*, *61*(8), 1975–1983. https://doi.org/10.1016/j.asr.2018.
- Springer, T. A., Beutler, G., & Rothacher, M. (1999). A new solar radiation pressure model for GPS satellites. GPS Solutions, 2(3), 50–62. https://doi.org/10.1007/PL00012757
- Standish, E. M., & Williams, J. G. (1992). Orbital ephemerides of the Sun, Moon, and planets. *Explanatory supplement to the astronomical almanac*, 1992, 279–323
- Svehla, D., & Rothacher, M. (2004). Formation flying of leo satellites using GPS. Eos Trans Am Geosci Union AGU 85(47), Fall Meet. Suppl. Abstract SF53A-0735. 2004, 13–17 December 2004, San Francisco, US
- Svehla, D., & Rothacher M. (2005). First LEO satellite constellation based on GPS. AGU Fall Meeting Abstracts 2005, A51F-01, San Francisco, US
- Svehla, D. (2018). Geometrical theory of satellite orbits and gravity field.
  SpringerNature, (537 pages) ISBN Hardcover: 978–3–319–76872–4, ISBN e-book: 978–3–319–76873–1 http://www.springer.com/gp/book/97833 19768724
- Tang, C., Hu, X., Zhou, S., Liu, L., Pan, J., Chen, L., Guo, R., Zhu, L., Hu, G., Li, X., He, F., & Chang, Z. (2018). Initial results of centralized autonomous orbit determination of the new-generation BDS satellites with inter-satellite link measurements. *Journal of Geodesy, 92*(10), 1155–1169. https://doi.org/10.1007/s00190-018-1113-7
- Xia, F., Zhou, S., Li, Z., Jiang, N., & Hu, X. (2024). Analysis of long-term distributed autonomous orbit determination for BeiDou-3 satellites. *Journal of Geodesy*, 98, 95. https://doi.org/10.1007/s00190-024-01857-y
- Xie, X., Geng, T., Zhao, Q., Cai, H., Zhang, F., Wang, X., & Meng, Y. (2019). Precise orbit determination for BDS-3 satellites using satellite-ground and intersatellite link observations. GPS Solutions, 23(2), 40. https://doi.org/10. 1007/s10291-019-0823-5

- Yang, L. (2019). The CentiSpace-1: A leo satellite-based augmentation system. In: 14th meeting of the international committee on global navigation satellite systems, pp. 12.
- Yang, Y., Ren, X., Jia, X., & Sun, B. (2023). Development trends of the national secure PNT system based on BDS. *Science China Earth Sciences*, *66*(5), 929–938. https://doi.org/10.1007/s11430-022-1069-7
- Yang, Z. (2022). Research on the Method for Integrated Orbit Determination and Clock Estimation of LEO and GNSS satellites. Wuhan University.
- Yu, F., He, Z., & Xu, N. (2019). Autonomous navigation for GPS using inter-satellite ranging and relative direction measurements. Acta Astronauta, 160, 646–655. https://doi.org/10.1016/j.actaastro.2019.03.011
- Zhang, Y. (2005). Study on autonomous navigation of constellation using intersatellite measurement. Wuhan University.

# **Publisher's Note**

Springer Nature remains neutral with regard to jurisdictional claims in published maps and institutional affiliations.